https://doi.org/10.5194/acp-2022-761
Preprint. Discussion started: 17 November 2022

Atmospheric Chemistry and Physics Discussions

Ice Nucleating Particles in Northern Greenland: annual cycles, biological contribution and parameterizations

Kevin C. H. Sze[1], Heike Wex[1], Markus Hartmann[1,3], Henrik Skov[2], Andreas Massling[2], Diego Villanueva[4], and Frank Stratmann[1]

[1]Experimental Aerosol and Cloud Microphysics, Leibniz Institute for Tropospheric Research, Leipzig, Germany
[2]iClimate, Arctic Research Center, Department of Environmental Science, Aarhus University, Roskilde, Denmark
[3]now at: Atmospheric Science, Department of Chemistry & Molecular Biology, University of Gothenburg, Gothenburg, Sweden
[4]Institute for Atmospheric and Climate Science, ETH Zürich, Zurich, 8092, Switzerland

Correspondence: Kevin C.H. Sze (sze@tropos.de) and Heike Wex (wex@tropos.de)

Abstract. Ice nucleating particles (INPs) can initiate ice formation in clouds at temperatures above −38°C through heterogeneous ice nucleation. As a result, INPs affect cloud microphysical and radiative properties, cloud life time and precipitation behavior and thereby ultimately the Earth's climate. Yet, little is known regarding the sources, abundance and properties of INPs especially in remote regions such as the Arctic. In this study, two-year-long INP measurements (from July 2018 to September 2020) at Villum Research Station (VRS) in Northern Greenland are presented. A low-volume filter sampler was deployed to collect filter samples for off-line INP analysis. An annual cycle of INP concentration (N_{INP}) was observed and the fraction of biogenic INPs was found to be higher in snow-free months and lower in months when the surface was snow-covered. Samples were categorized into three different types based only on the slope of their INP spectra, namely into summer, winter and mix type. For each of the types a temperature dependent INP parameterization was derived, clearly different depending on the time of the year. Winter and summer type occurred only during their respective seasons and were seen 60% of the time. The mixed type occurred in the remaining 40% of the time throughout the year. April, May and November were found to be transition months. A case study comparing April 2019 and April 2020 was performed. The month of April was selected because a significant difference in N_{INP} was observed during these two periods, with clearly higher N_{INP} in April 2020. N_{INP} in the case study period revealed no clear dependency on either meteorological parameters or different surface types which were passed by the collected air masses. Overall, the results suggest that the coastal regions of Greenland were main sources of INPs in April 2019 and 2020, most likely including both local terrestrial and marine sources. In parallel to the observed differences in N_{INP}, also a higher cloud ice fraction was observed in satellite data for April 2020, compared to April 2019.

1 Introduction

The Arctic is known to be one of the most sensitive regions on Earth, where climate change takes place in an unexpectedly intense pace (Cohen et al., 2014; Serreze and Barry, 2011; Morrison et al., 2012). In the last two decades, the Arctic near-surface air temperature has increased almost four times as fast as that of the rest of the globe (Rantanen et al., 2022). This

https://doi.org/10.5194/acp-2022-761
Preprint. Discussion started: 17 November 2022


Atmospheric Chemistry and Physics Discussions

phenomenon is usually referred to as Arctic Amplification (AA) (Wendisch et al., 2017; Cohen et al., 2014). Different effects and feedbacks such as surface albedo effect, water vapour, lapse rate and cloud feedback, have been studied and identified as potential contributors to AA (Wendisch et al., 2017). However, the combined effects and their relative importance to the Arctic region, as well as their influence on the mid-latitude weather, are still unclear (Pithan and Mauritsen, 2014; Cohen et al., 2020). Aerosol particles are an important component in the climate system. They can directly scatter and/or absorb radiation (Myhre et al., 2013; Boucher et al., 2013), and affect the energy budget of the Arctic boundary layer by altering the microphysical properties of clouds (Morrison et al., 2012; Pruppacher and Klett, 2010). Arctic clouds are often low-level, persistent and form stratiform layers (Shupe et al., 2006). They tend to cause a net warming effect for the underlying surface in comparison to clear sky condition, due to the upward longwave radiation reflected downward by the cloud (Intrieri et al., 2002; Shupe and Intrieri, 2004). This can increase the sea ice melt (Vavrus et al., 2011), and facilitate biological activities in the ocean, which then can contribute to and change the Arctic aerosol population (Creamean et al., 2019; McCluskey et al., 2017). Analogous to the marine environment, it is expected that the terrestrial ecosystem will respond to longer snow-free periods with enhanced biological activity (Cooper, 2014). This may lead to more primary biological aerosol particles directly emitted from plants, such as pollen and spores. Also, exposure of non snow-covered surfaces to the atmosphere will enhance emission of soil dust, that can largely contribute to ice-nucleating particles (INPs). As the Arctic is warming, the permafrost is also expected to thaw, promoting microbial metabolic activity in the soil (Wild et al., 2019; Schuur et al., 2015), which then could be mobilized in the atmosphere as well (Creamean et al., 2020).

Clouds in the Arctic are usually mix-phased (Shupe et al., 2006), i.e. contain both, supercooled liquid droplets and ice crystals. Primary ice formation in the atmosphere can happen via homogeneous nucleation at -38°C or below, or via heterogeneous nucleation where aerosol particles, the already mentioned INPs, act as catalysts at any temperature below 0°C (Vali et al., 2015). Immersion freezing is arguably the most relevant freezing mechanism in the Arctic mix-phased clouds (MPCs) regime, which requires INPs immersed into cloud droplets (Boer et al., 2011; Hande and Hoose, 2017). By inducing the ice formation in MPCs, the presence of INPs can alter the amount and size of liquid droplets and ice crystals in a cloud through e.g. the Wegener–Bergeron–Findeisen process. Connected to this, for Arctic mixed-phase clouds at temperatures above -10°C, it was recently observed that they contain heterogeneously formed ice 2 to 6 times more often when they were coupled to the surface, compared to decoupled clouds (Griesche et al., 2021). Ultimately, INPs affect the radiative properties, life time and precipitation formation in the clouds (Kanji et al., 2017; Hoose and Möhler, 2012; Murray et al., 2012).

The ability of aerosol particles acting as INPs largely depends on their size, morphology, composition and source (Hoose and Möhler, 2012). However, correlating INP concentration with physical properties of the bulk aerosol was shown to be difficult (Welti et al., 2018; Li et al., 2022). Aerosol particles from materials such as mineral dust, sea salt, volcanic ash, soot and biological sources have been shown to serve as INPs in different temperature regimes (Petters et al., 2009; Murray et al., 2012; DeMott et al., 2015; Maters et al., 2019; O'Sullivan et al., 2018; Szyrmer and Zawadzki, 1997). Particularly, mineral dust and biological material are the two most abundant INPs in the atmosphere (Coluzza et al., 2017; DeMott et al., 2003). Mineral dust is known to be more relevant at lower temperatures compared to biological INPs, which are relevant at higher temperatures. Pure mineral dust can show ice activity at around -15°C (Kanji et al., 2017), with submicron size particles shown to nucleate

https://doi.org/10.5194/acp-2022-761
Preprint. Discussion started: 17 November 2022


Atmospheric Chemistry and Physics Discussions

ice efficiently below -20°C (Augustin-Bauditz et al., 2014). In general, biological entities such as fungal spores, pollen, algae and lichen can nucleate ice above -20°C (O'Sullivan et al., 2018). And certain bacteria, such as Pseudomonas syringae, are the most efficient INPs studied so far, which can show ice activity at temperatures close to 0°C (Maki et al., 1974). Atmospheric dust particles can serve as carriers for biogenic material, enabling ice nucleation at a much higher temperature compared to dust alone (Augustin-Bauditz et al., 2014; O'Sullivan et al., 2014; Conen et al., 2011). Although biological INPs are rare in the atmosphere, in a remote environment such as the Arctic where particle concentrations are generally low, they potentially take up a large proportion among the INP population (Creamean et al., 2019), particularly among the highly ice active INPs. Consequently, biological INPs are crucial to cloud phase, and eventually can have a large impact on the climate. However, little is known about the sources and temporal variation of biological INPs in the Arctic.

Efforts have been made in the past concerning the determination of sources, abundance and properties of Arctic INPs. Several studies have reported that both terrestrial and marine environments can contribute to INPs in the Arctic, at -15°C and above. However, most conclusions are based on short-term campaign-wise activities. Bigg and Leck (2001) measured INPs on a ship cruise around the central Arctic Ocean from July to September 1996 and reported a decrease of INP concentration during the period. Bacteria and fragments of marine organisms were suggested to be the source of INPs. Bigg (1996) reported sources from open ocean during a cruise from August to October, and even explicitly mentioned that terrestrial sources are of minor importance. Hartmann et al. (2021) also showed the possibility of airborne INPs originating from a local marine, probably biological source. A study based on airborne measurements showed that long-range transport does most likely not contribute to the INP population in the Arctic (Borys, 1989), while sources are likely local, such as cracks, open leads and polynyas in sea ice (Hartmann et al., 2020; Kirpes et al., 2019). On the other hand, it has been shown that the Arctic aerosol in general is strongly influenced by long-range transport from outside the Arctic especially from January through April (Schmale et al., 2021; Massling et al., 2015; Lange et al., 2018). Wilson et al. (2015) and Irish et al. (2017) reported enhanced ice activity of samples collected from sea surface microlayer and bulk water in the Arctic Ocean. It was suggested that such activity relate to heat-labile biological material and organic material, with diameters smaller than 0.2μm. Effort has also been made to connect these materials with biological processes such as phytoplankton blooms, which were found to be directly associated with biologically derived INPs (Creamean et al., 2019; Schnell and Vali, 1976; Zeppenfeld et al., 2019). These INPs in the sea can be eventually released into the air among sea spray aerosols through processes such as bubble bursting (DeMott et al., 2016; Wilson et al., 2015; Creamean et al., 2019).

Apart from marine sources, samples collected at coastal sites can also be influenced by terrestrial sources as well (Si et al., 2018). Few studies also found indications for a seasonal cycle, which showed higher INP concentration during summer time, and lower INP concentration during winter time (Šantl Temkiv et al., 2019; Wex et al., 2019; Creamean et al., 2018). While the studies presented above see marine sources as the main INP sources in the Arctic, there are several studies that have pointed out that terrestrial sources can contribute to the INP population in the Arctic. Conen et al. (2016) showed that decaying leaf litter emitting biological material could be a strong source of INPs to the Arctic boundary layer, at a coastal measurement site in Norway (69°55'45" N, 22°48'30" E). Another study also pointed out that ice activity of sediment material from a glacial outwash plain from Svalbard is governed by a small amount of biological material, causing high ice activity and leading to

https://doi.org/10.5194/acp-2022-761
Preprint. Discussion started: 17 November 2022


Atmospheric Chemistry and Physics Discussions

INPs important under conditions relevant for MPCs formation (Tobo et al., 2019). This is one example for mineral dust acting as carrier for biological INPs. Icelandic mineral dust was shown to largely contribute to the INP population at mid to high latitudes by using aircraft-collected samples and a global aerosol model (Sanchez-Marroquin et al., 2020). These all highlight the importance of biological INPs, especially in the fast changing Arctic, where snow and sea ice cover are expected to decline in the upcoming years, which will lead to increased biological activity in the Arctic and thus potentially provide significant amounts of biological material as mentioned above.

To date, a limited number of studies have evaluated INPs at coastal and marine environments in the Arctic, although recently MOSAiC, a comprehensive measurement campaign on a research vessel, spending over one year in the Arctic, was conducted (Shupe et al., 2022), from which first INP data have been published (Creamean et al., 2022). Still, quantitative insights about the sources and properties of INPs are still lacking. Dedicated long term measurements in the Arctic region are scarce. They are needed to understand what drives and influences the seasonal changes of the Arctic INP population, as well as to provide robust constrains for the abundance of Arctic INPs and reduce the uncertainty of the aerosol-cloud-interaction in climate models (Murray et al., 2021, 2012). A recent model study showed that a parameterization that delivers low INP concentrations during summer weakens the cloud feedback, which further elaborates to the importance of INPs to AA and the need for parameterizations that are representative throughout the year (Tan et al., 2022).

In this study, a two-year-long time series of INP measurements at Villum Research Station (VRS) in Northern Greenland (81°36' N, 16°40' W) is presented, of which the second year coincided with the time of the MOSAiC expedition (Shupe et al., 2022). Filter samples taken at VRS were evaluated with well established off-line methods. An observed seasonal variation of INP concentrations and possible INP sources is discussed. A seasonally varying parameterization for INP concentrations is derived. Two shorter time periods were selected for a case study and investigated in more detail. To our knowledge, this is the first perennial time series of INP measurements in Greenland and the high Arctic north of 80°N.

2 Materials and methods

2.1 Sampling site and filter sampling

Filter sampling has taken place at remote Villum Research Station (VRS) in Northern Greenland (81°36' N, 16°40' W). A low volume aerosol sampler (LVS; DPA14 SEQ LVS, DIGITEL Elektronik AG, Volketswil, Switzerland) with a PM_{10} inlet (DPM10/2.3/01, DIGITEL Elektronik AG, Volketswil, Switzerland) has been operated at the station since March, 2018. The sampler was placed inside of the research station, with the inlet above the roof at approximately 5 m above ground level. It was operated with an average volumetric flow rate of 21 L min^{-1}. This flow rate is less than the nominal flow rate for the inlet used, hence the effective cut-off diameter is approximately 13.51 μm. An automatic filter changing function was utilized, which allowed unsupervised sampling of multiple subsequent samples with sampling periods of 3.5 days each. In addition to these two filters per week, every week a field blank filter was taken. The field blank filters were handled in the same manner as sampled filters, but without actual air flow sucked through them. In a normal routine 3 clean filters were placed inside the sampler weekly. Similarly, also weekly, two sampled and one blank filter were retrieved and packed up for frozen storage.

https://doi.org/10.5194/acp-2022-761
Preprint. Discussion started: 17 November 2022


Atmospheric Chemistry and Physics Discussions

Samples were collected on polycarbonate pore filters (Nuclepore®, Whatman™; 47mm diameter). After collection, filters were stored at around −20°C on site. The collected filters were transported within a cooled container at −20°C to the Leibniz Institute for Tropospheric Research (TROPOS), Germany where the samples were then stored until analysis. A summary of the amount of filters analyzed and presented for each month in this study is shown in the appendix in Table A1.

2.2 INP analysis

2.2.1 Sample preparation

For analysis, a filter was placed in an individual centrifuge tube (50 mL, Cellstar®, sterile, Greiner Bio-One, Kremsmünster, Austria), immersed with 3 mL of ultra-pure water (type 1; Direct-Q® 3 water purification system, Merck Millipore, Darmstadt, Germany). The tubes were then shaken with a flask shaker for 20 minutes in order to wash off all the particles from the filters into the water. A total volume of 100 μL liquid sample was first extracted for analysis using the Leipzig Ice Nucleation Array (LINA; see Section 2.2.2). Then, to the remaining 2.9 mL liquid sample 3.1 mL ultra-pure water were added to a total volume of 6 mL liquid sample, which was then analyzed with the Ice Nucleation Droplet Array (INDA; see Section 2.2.3). The purpose of this procedure is to ensure that there is sufficient amount of liquid sample for analysis with INDA, while at the same time diluting the sample as little as possible.

2.2.2 Leipzig Ice Nucleation Array (LINA)

LINA is a droplet freezing device, based on the design of the Bielefeld Ice Nucleation ARraY (BINARY) by Budke and Koop (2015). The array consists of 90 droplets with a volume of 1 μL each. The droplets are positioned on a circular hydrophobic glass slide with a diameter of 40 mm. Each droplet is placed in an individual compartment separated by an aluminium grid, covered up with another glass slide. This is to ensure that the droplets do not interact with each other during the freezing process and to minimize the possibility of evaporation. The droplets are then cooled on a Peltier element in a cooling stage (LTS120, Linkam Scientific Instruments, Waterfield, UK) with a cooling rate of 1°C min^{-1} (with a temperature resolution of about 0.1°C). The cooling is assisted by a cryogenic water circulator (F25-HL, Julabo, Seelbach, Germany), in order to enable low temperatures close to the point of homogeneous freezing at −38°C. A thin layer of squalene oil is added between the cooling stage and the hydrophobic glass slide carrying the droplets, to ensure proper heat transfer to the Peltier element. The whole Peltier element is encased in a sealed chamber, with a steady flow of dry air going through the chamber and above a viewing window in order to avoid any condensation. The whole setup is illuminated by a dome shape light source (SDL-10-WT, MBJ-Imaging GmbH, Hamburg, Germany) from above. A camera (acA2040-25gm - Basler ace, Basler AG, Ahrensburg, Germany) placed inside the dome records images every 6 seconds during the cooling process. The images are then evaluated with a custom software to derive the number of frozen droplets in each image. With that, frozen fraction $f_{ice}(T)$ (see Section 2.2.5 for definition), can be determined at each temperature.

https://doi.org/10.5194/acp-2022-761
Preprint. Discussion started: 17 November 2022


Atmospheric Chemistry and Physics Discussions

2.2.3 Ice Nucleation Droplet Array (INDA)

INDA is a droplet freezing device inspired by Conen et al. (2015). Instead of individual Eppendorf tubes as used by Conen et al. (2015), a PCR (Polymerase Chain Reaction) plate was utilized as introduced by Hill et al. (2016). The PCR plate (Brand GmbH & Co. KG, Wertheim, Germany) consists of 96 wells, and each well is filled with a 50μL aliquot of the liquid sample. In this study, typically two liquid samples were evaluated in one plate (i.e. f_{ice}(T) was determined based on 48 wells). The plate is then sealed with a transparent foil on top, placed in a plate holder, and the wells of the PCR plate are immersed into the ethanol bath of a cryostat (FP45-HL, Julabo, Seelbach, Germany). In contrast to LINA, the light source that illuminates the sample aliquots is situated below the PCR plate. The cryostat bath is then cooled at a cooling rate of $1°C\,min^{-1}$, with the camera (DMK 33G445, The Imaging Source Europe GmbH, Bremen, Germany) above taking an image for every $0.1°C$ step. The images are then evaluated by a custom software that counts the number of frozen sample aliquots at a certain temperature which yields at the end the frozen fraction f_{ice}(T). Compared to LINA, INDA uses sample aliquots that are a factor of 50 larger (50 μL vs. 1 μL), allowing measurements of INPs in a different but overlapping concentration range.

2.2.4 Thermal treatment for heat-labile INPs

Thermal treatment was performed in order to evaluate the presence of heat-labile INPs such as proteinaceous biological material (Hill et al., 2016). The ice nucleation ability of biological INPs primarily originates from proteins, which denature at certain temperatures, reducing their ability to nucleate ice. However, it should be noted that not all biological INPs are equally sensitive to heat. Nevertheless, overall heat-lability is thought to be more associated with biological INPs than mineral INPs, and we will use the term biological INP in this study to refer to heat-labile INP. To test heat lability, the thermal treatment described in the following was applied to the same PCR plates that were used in the INP measurements with INDA. The PCR plate was placed in an oven (VL 56 Prime, VWR, Radnor, Pennsylvania, U.S.A.) and typically heated up to $90°C$ and held at that temperature for 1h. Once the sample cooled down to room temperature its ice activity was assessed again with the INDA setup. Due to technical reasons, some samples were only heated up to $85°C$. As expected, by heating the ice activity of a sample decreases as biological compounds may become denatured. In order to assess the amount of biological INPs, the INP spectra of the heated samples were compared with the unheated samples in order to quantify the fraction of biological INPs in the sample (see Section 2.2.7).

2.2.5 Deriving INP number concentration N_{INP}

The cumulative number concentration of INPs (N_{INP}) per air or water volume as a function of temperature can be calculated according to Vali (1971):

$$N_{INP}(T) = -\frac{ln(1 - f_{ice}(T))}{V} \quad (1)$$

https://doi.org/10.5194/acp-2022-761
Preprint. Discussion started: 17 November 2022

Atmospheric Chemistry and Physics Discussions

with $f_{\mathrm{ice}}(T) = \frac{N(T)}{N_{\mathrm{total}}}$, where N(T) is the number of frozen droplets at a specific temperature. For LINA, N_{total} is 90, while for INDA, N_{total} is 48, i.e., the total number of examined droplets. V is the reference volume and is defined as:

$$V = \frac{V_{\mathrm{flow}}}{V_{\mathrm{water}}} \cdot V_{\mathrm{droplet}} \tag{2}$$

where V_{flow} is the air volume sampled through the filter, V_{water} is the volume of washing water (LINA: 3 mL; INDA: 6.21 mL) and V_{droplet} is the volume of each droplet (LINA: 1μL; INDA: 50μL). INP number concentration per water volume $N_{\mathrm{INP,water}}$ was also calculated in order to evaluate the consistency between LINA and INDA (see Appendix A1). V here was defined as:

$$V = \frac{V_{\mathrm{droplet}}}{V_{\mathrm{water}}} \tag{3}$$

All spectra of untreated samples shown in this study are merged from the individual LINA and INDA spectra of the respective sample. For simplicity, the INP number concentration per air volume after merging is denoted as N_{INP}. See Appendix A1 for detailed description regarding the merging procedures.

2.2.6 Uncertainty of N_{INP} and detection limit

Uncertainties in the derived N_{INP} due to the underlying Poisson distribution are assessed based on a formula by Agresti and Coull (1998), which yields the 95% confidence interval for f_{ice}(T):

$$\left(f_{\mathrm{ice}} + \frac{z_{a/2}^2}{2n} \pm z_{a/2} \sqrt{[f_{\mathrm{ice}}(1-f_{\mathrm{ice}}) + z_{a/2}^2/(4n)]/n} \right) / (1 + z_{a/2}^2/n), \tag{4}$$

where n is the droplet number, and $z_{a/2}$ is the standard score at a confidence level $a/2$, which for a 95% confidence interval is 1.96. This approach was successfully applied to INP analysis by several previous studies such as Hill et al. (2016), Hartmann et al. (2021) and Gong et al. (2020). The lower and upper values of the interval of f_{ice}(T) were then converted into N_{INP} by using equation 1. Error bars of LINA and INDA spectra are exemplarily shown in Fig A3 for every 1°C step, but for the sake of readability not shown in other figures. N_{INP} could not be determined at those temperatures for which the detection limits were reached, i.e. when f_{ice}(T) was 0 or 1, where equation 1 is not applicable to calculate the corresponding N_{INP}. In this situation, f_{ice}(T) were assumed to be $\frac{1}{N_{\mathrm{total}}}$ and $\frac{N_{\mathrm{total}}-1}{N_{\mathrm{total}}}$, for f_{ice}(T) = 0 and f_{ice}(T) = 1, respectively. With the median sampling air volume (105839 L) and typical droplets number N_{total} (90 for LINA; 48 for INDA), the overall lower and upper detection limits of N_{INP} are $2.5 \cdot 10^{-5}$ and $1.3 \cdot 10^{-1}$ per liter of air respectively.

2.2.7 Quantifying the contribution of biological INP

As described in Section 2.2.4, samples underwent thermal treatment for testing the presence of heat-labile INPs. The amount of heat-labile INP can be seen as a proxy for the amount of biological INPs in a sample. In order to quantify the presence of biological INPs in the samples, a similar analysis was conducted as in Gong et al. (2022). The atmospheric INP number concentration of the heated samples ($N_{\mathrm{INP,air}}^{\mathrm{heated}}$) and its corresponding unheated samples (i.e. the full spectrum, see Appendix A1 for details of merging procedure) at each temperature were used to derive the bio-ratio N_{bioratio} using the followoing equation:

https://doi.org/10.5194/acp-2022-761
Preprint. Discussion started: 17 November 2022


Atmospheric Chemistry and Physics Discussions

$$N_{\mathrm{bioratio}}(T) = 1 - \frac{N^{\mathrm{heated}}_{\mathrm{INP,air}}(T)}{N_{\mathrm{INP}}(T)} \tag{5}$$

Based on this quantification, samples containing a higher fraction of biological INPs show values close to 1, while samples containing a lower fraction show values close to 0. Respective results are discussed in Section 3.4.

2.2.8 Back-trajectory calculations, satellite remote sensing data, and meteorological parameters

In order to locate potential INP sources, the HYbrid Single-Particle Lagrangian Integrated Trajectory (HYSPLIT; Stein et al. (2015)) model was used to calculate 5-day air mass backward trajectories for selected times. GDAS1 (Global Data Assimilation System; 1°latitude /longitude; 3-hourly) meteorological fields from the National Centers for Environmental Prediction (NCEP) were used as input data of the back-trajectory calculation. Trajectories were initiated at the coordinates of VRS (81°36' N, 16°40' W) 50 m above ground level every 3 h. This low starting height is justified by an almost constant inversion height at about 100 m and another about 230 m (Gryning et al., 2022).

Sea ice concentration maps along the path of the back-trajectories were derived from the ASI sea ice concentration product from the University of Bremen (available at https:seaice.uni-bremen.de; Spreen et al. (2008)). The daily sea ice concentration maps have a grid resolution of 6.25 km.

Meteorological parameters such as wind direction, wind speed, relative humidity, surface temperature, pressure, radiation and snow depth are measured continuously at VRS (available at https://villumresearchstation.dk/data). The snow depth was studied and used to distinguish snow-free and snow-covered months (see Section 3.1 and 3.4). All aforementioned meteorological parameters were investigated in a case study (See Section 3.5). In addition, high, medium, low and total cloud cover, cloud base and boundary layer height, total column cloud liquid and ice water content, total precipitation were retrieved from ERA5 reanalysis (Hersbach et al., 2018). Data were then linearly interpolated to the coordinates of VRS, and are discussed in the same section.

2.2.9 Ice cloud fraction from satellite data for case study

For a case study we used cloud ice fractions derived from satellite data, namely the CALIPSO Lidar Level 2 Vertical Feature Mask (VFM) Version 4.20. In this product, to determine the cloud phase, the ratio between depolarization ratio and attenuated backscatter is used (Hu et al., 2007, 2009; Avery et al., 2020).

Following Villanueva et al. (2021), for each day of the examination period, which included all of April 2019 and 2020, we merged both the ascending and descending overpasses temporally from 0 to 24 UTC. Only the top cloudy pixels from each instant vertical profile were included. Using the temperature at cloud top, we assigned each pixel to a 3 K temperature bin between -42°C and 3°C. We regrided all three products to a $2° \times 30°$ (lat × lon) grid by averaging the binary cloud-phase flags contained inside each gridbox.

https://doi.org/10.5194/acp-2022-761
Preprint. Discussion started: 17 November 2022

Atmospheric Chemistry and Physics Discussions

3 Results and discussion

3.1 Atmospheric INP concentrations in the Arctic

A time series of atmospheric INP concentrations at three different selected temperatures (i.e. at -12°C, -16°C and -20°C) is shown in Fig. 1 (the full spectra of all samples are shown in Fig. A4 in the Appendix). The gray-shaded areas in Fig. 1 indicate the period when the snow depth at VRS was below 0.8m, which was used as the threshold to indicate beginning and end of the snow melt season. Hereafter the time period with a snow depth below the threshold is referred to as snow-free months, while the remaining period is called snow-covered months (a time series of the snow depth can be seen in Fig. A6). At -12°C and -16°C, a clear seasonal cycle is observed, where comparably high N_{INP} are found in the snow-free months, and lower N_{INP} in the snow-covered months. This is in line with results shown in several previous studies (Wex et al., 2019; Šantl Temkiv et al., 2019; Creamean et al., 2018). N_{INP} at these three temperatures span between 1 to 2 orders of magnitude, with the variability higher at higher temperatures, and lower at lower temperatures, as can be seen in Table 1. This difference in variability may be

Table 1. Percentiles of N_{INP} (10^{th} to 90^{th}) at $-12°$, $-16°$ and -20°C for the whole period, snow-free months and snow-covered months, respectively.

	$N_{INP}(-12°C)$	$N_{INP}(-16°C)$	$N_{INP}(-20°C)$
Whole period	1.9×10^{-4} to 1.1×10^{-2}	7.4×10^{-4} to 3.3×10^{-2}	3.9×10^{-3} to 7.4×10^{-2}
Snow-free months	6.2×10^{-4} to 1.5×10^{-2}	2.3×10^{-3} to 4.1×10^{-2}	3.7×10^{-3} to 7.5×10^{-2}
Snow-covered months	1.6×10^{-4} to 9.0×10^{-3}	6.4×10^{-4} to 2.4×10^{-2}	4.1×10^{-3} to 7.1×10^{-2}

attributed to the type of aerosol particles active as INPs at the different temperatures. At -15°C or above, biological material is anticipated to act as efficient INP and to contribute to the majority of the INP population at this temperature. Local sources were proposed in the past for these INPs. It is also known that local biological processes are more pronounced in summer compared to in winter. At around -16°C and below, long-range transported INPs, most likely mineral dust, can start to show ice activity, while biological material persist to behave as INPs and still contributes to the majority of all INP. For temperatures below roughly -20°C, mineral dust can most likely dominate the whole INP population. This background of INPs may reduce the variation of the INP concentrations, as seen in Fig. 1 (Creamean et al., 2019; O'Sullivan et al., 2018; Kanji et al., 2017; Augustin-Bauditz et al., 2014). The thermal treatment of samples points towards the existence of biological INPs at higher temperatures, which is discussed in more detail in Section 3.4. It should also be mentioned that the upward and downward pointing triangles in Fig. 1 indicate N_{INP} above and below the detectable range of the used freezing assays, respectively. The symbols were added in order to emphasize that INPs exist above or below the detection range for the respective sample. Looking at Fig 1, it can also be seen that in April 2020, N_{INP} are much higher than in April 2019. To elucidate possible reasons for this difference, a case study of these two months is presented in Section 3.5.

https://doi.org/10.5194/acp-2022-761
Preprint. Discussion started: 17 November 2022

Atmospheric Chemistry and Physics Discussions

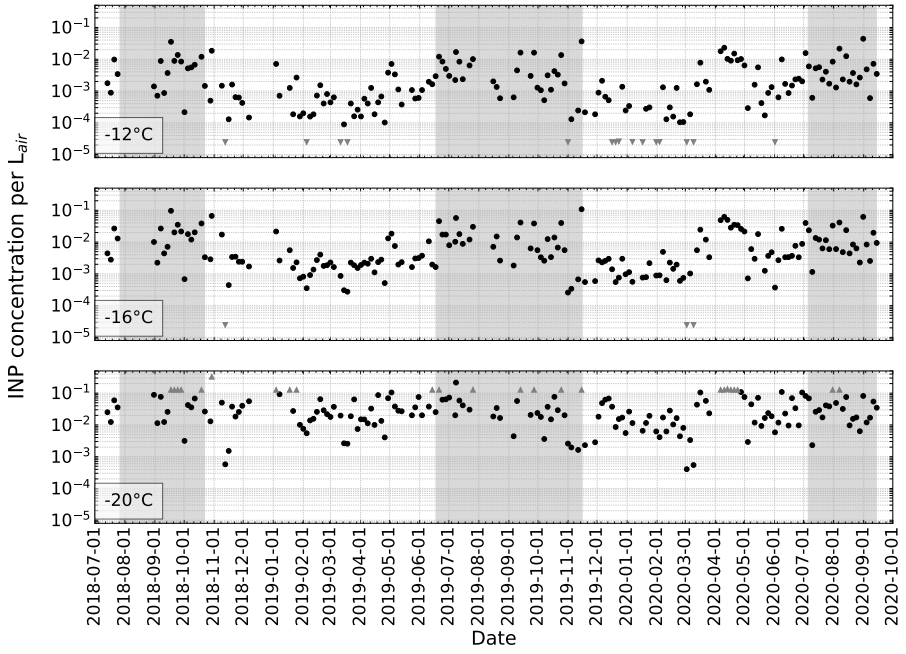

Figure 1. Time series of N_{INP} at -12°C, -16°C and -20°C. Circles represent measured INP concentrations, while upward and downward pointing triangles indicate that samples have INP concentrations above or below the detectable range, respectively. Note that the detection limit varies depending on the air volume sampled on the filter. The gray areas show periods when snow depth measured at Villum Research Station (VRS) was below 0.8m.

3.2 Spectra characterization and frequency distribution of N_{INP}

INP spectra varied significantly throughout the two-year-long data-set. To see if there were systematic changes, a characterization of the spectra was carried out aiming at the division of the spectra in groups with distinct features. Just from plotting all spectra, it became obvious that they generally followed one of the three types of spectra exemplified in Fig. 2. It was particularly striking, that spectra with generally lower INP concentrations were steeper, while spectra featuring higher concentrations exhibit more shallow slopes. Spectra with low concentrations generally followed a temperature (T) dependent trend roughly proportional to $e^{-0.6 \cdot T}$, while those with high concentrations roughly followed $e^{-0.3 \cdot T}$ below approximately -10°C. Those spectra in between showed shallower slopes at higher temperatures and steeper slopes at lower temperatures. The slopes in the exponential decay terms given above, -0.6 and -0.3, bring to mind those from two well-known older publications, Fletcher (1962) and Cooper (1986), respectively. Their respective INP parameterizations are often used in atmospheric models. It should be noted that Fletcher (1962) reported the value of -0.6 as the usual value, but commented that values between -0.4 and -0.8 were still common. In Cooper (1986), a selection of previously made measurements from literature was examined. However, it was not well described based on what criteria certain data was included or rejected. Still, when sighting this literature, it can be seen that data at higher temperatures up to -5°C was included in Cooper (1986), while Fletcher (1962) used data only

https://doi.org/10.5194/acp-2022-761
Preprint. Discussion started: 17 November 2022

Atmospheric Chemistry and Physics Discussions

downward from -10°C and mostly even below -15°C. Possibly, the presence of biological INPs active at higher temperatures, included for samples selected by Cooper (1986), but missing in the samples included in Fletcher (1962), was responsible for the differing parameterizations given in these two publications. In the present study, the reasoning behind this hypothesis will become clearer in the following.

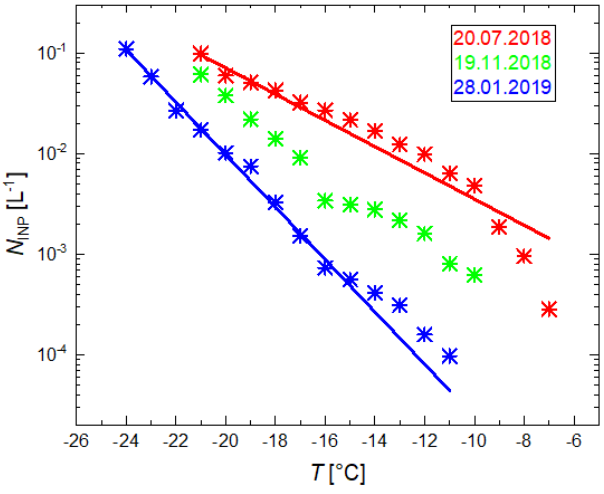

Figure 2. Three exemplary INP spectra together with fits based on exponential decay with a slope of -0.6 for the sample with sampling end date of 20190128 and -0.3 for the sample with sampling end date of 20180720.

Based on the above described observations for our own data-set, an automated discrimination of samples into three different types of spectra was aimed at. For that, each INP spectrum was fitted twice with a curve describing an exponential decay following ($A \cdot e^{s \cdot T}$). One fit was based on a fixed slope, s, of -0.6 and the second on a fixed slope of -0.3 resulting in only one free parameter, A, to be fitted. All available measured data across all temperatures, T, were included. These two slopes were chosen, as they are commonly used in models, as described above, and they fit well on all of the spectra with low or high concentrations, respectively. A number of parameters resulting from these fits were examined, such as the resulting fit-factors A and the root mean square differences between the measured spectra and the fits. Some parameters were clearly different between samples with high and low concentrations. The normalized least square difference was chosen for an automated discrimination, both obtained in the temperature range between -15°C and -12°C:

$$\mathrm{P1} = \sum_{T=-15}^{-12} \frac{(Ae^{-0.6 \cdot T} - N_{\mathrm{INP}})^2}{(Ae^{-0.6 \cdot T})^2} \tag{6}$$

and

$$\mathrm{P2} = \sum_{T=-15}^{-12} \frac{(Ae^{-0.3 \cdot T} - N_{\mathrm{INP}})^2}{(Ae^{-0.3 \cdot T})^2} \tag{7}$$

https://doi.org/10.5194/acp-2022-761
Preprint. Discussion started: 17 November 2022


Atmospheric Chemistry and Physics Discussions

where P1 indicates, how well the steeper slope of -0.6 describes the measured values in the temperature range from -15°C to -12°C, and P2 indicates the same for the less steep slope of -0.3. Samples for which the steeper slope of -0.6 fits well in the temperature range from -15°C to -12°C have a comparably low P1. All samples for which P1 $< 5 \times 10^{-7}$ were labeled as *Fletcher type*. The lower the relation between the two parameters $\frac{\mathrm{P2}}{\mathrm{P1}}$ is, the better a spectrum is described by the less steep slope of -0.3. All samples for which $\frac{\mathrm{P2}}{\mathrm{P1}} < 2.5$ were labeled as *Cooper type*. These were the only two criteria which were used to group the data. All remaining spectra which did not fit to one of the two criteria made up roughly 40% of all samples. They typically had a less steep slope at temperatures above -17°C, and a steeper slope below. They were labeled as *mix type*. An overview of the spectra of all samples color-coded according to these types are shown in Fig. A5.

Next we assessed how often each of the three spectra types occurs in each month (Fig. 3). The *mix type* made up roughly 40% of all INP spectra in each month throughout the year. And roughly, the remaining 60% are almost exclusively *Fletcher type* in the winter months from December until March, and *Cooper type* in the summer months from June until October. April and May as well as November are intermediate months, in which all three types of spectra occur. The results shown in Fig. 3 corroborate that the automated discrimination described above was useful to discriminate between samples collected in typical summer and winter months. Hence, hereafter, we refer to the *Cooper type* spectra as *summer type*, and to the *Fletcher type* spectra as *winter type*.

After having categorized all spectra, the frequency distributions of $\mathrm{N_{INP}}$ at each measurement temperature from -7°C to -24°C for each of the three spectra types were investigated. For this, all spectra belonging to one type were combined, yielding frequency distributions of $\mathrm{N_{INP}}$ at each temperature, to which then log-normal fits were applied. This analysis was done based on Ott (1990), who suggested that log-normal distributions occur for atmospheric parameters, arising from successive random dilutions by different atmospheric processes during transportation from sources to measurement sites (as e.g., VRS). This has been adopted for INP concentrations at different temperatures by studies such as Schrod et al. (2020), Welti et al. (2018), and recently Li et al. (2022). Fig. 4 shows the frequency distributions as well as their respective log-normal fits for the same three temperatures that were selected for the $\mathrm{N_{INP}}$ time series (-12°C, -16°C and -20°C). It can be seen that at each temperature, the distributions fitted to data from the three different spectra types cover different $\mathrm{N_{INP}}$ ranges, with the maximum of the distribution, $X(T)$, show the highest value for the *summer type*, followed by the *mix type* and *winter type* at all temperatures. Another significant feature is that with decreasing temperature, the maximum of the distribution of each spectra type move closer together.

As seen in Fig. 4, at -12°C, the three types show a rather distinctive distribution. Based on previous studies which found a seasonal cycle of INPs, such as Wex et al. (2019), it can be assumed that this is due to the pronounced biological activity in the ocean or on land during the summer season, while in winter, local biological processes are lacking and long-range transported material such as mineral dust is the dominant background INP source. In mix type, neither of the two sources mentioned above is dominating, but both are contributing particles to the INP population. The transition from long-range transport to local and regional observations at Villum most likely happens in the months of April and May, or may already start as early as in March (Fenger et al., 2013). This explains the observation of INP spectra as mentioned above. At -16°C and further down at -20°C, the distributions of three types get closer to each other. While biological material dominates INP active at higher

https://doi.org/10.5194/acp-2022-761
Preprint. Discussion started: 17 November 2022

Atmospheric Chemistry and Physics Discussions

temperatures, mineral dust INPs become more noticeable and dominate the INP population when temperature gets lower. A common background of mineral dust particles throughout the year may exist, therefore bringing the distributions of three types closer together at lower temperatures, as seen in the lower panel in Fig. 4. In summer, when snow- and ice-covers retreat, local soil dust can be exposed to the atmosphere and contribute to the atmospheric aerosol load, contributing to the INPs population during this season.

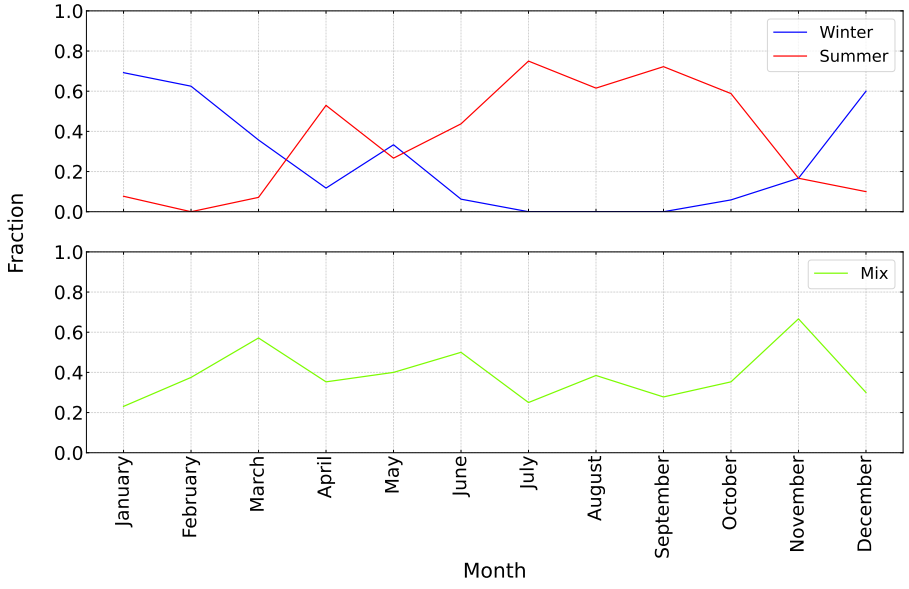

Figure 3. Time series of fractions of Fletcher type (winter) shown in blue, Cooper type (summer) shown in red, both in the upper panel, and shown in light green for mix type in the lower panel. Details of the amount of types in each month are shown in Table A2.

3.3 Arctic INP parameterization

It was shown in recent model studies that a temperature dependent INP parameterization is essential to accurately represent cloud properties in climate models (Hawker et al., 2021; Tan et al., 2022). In the present study, we developed three INP parameterizations, one for each of the three INP types described in Section 3.2. The parameterizations were derived by applying an ordinary least square (OLS) fit to the respective maximum, $X(T)$. All resulting temperature dependent INP parameterizations in this study follow the form of the equation below:

$$N_{\mathrm{INP}} = A \cdot e^{s \cdot T} \tag{8}$$

where A and s represent the y-intercept and the slope of the fit, respectively, T represents the temperature in °C, N_{INP} represents the atmospheric INP concentration per liter of air. Parameters of the parameterizations for summer, winter and mix type are shown in Table 2. In addition and for comparison purpose, fitting was also conducted using equation 8 with fixed slope values s of -0.6 and -0.3. Respective parameters are also shown in Table 2 as reference. As discussed above, these

https://doi.org/10.5194/acp-2022-761
Preprint. Discussion started: 17 November 2022

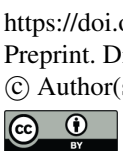

Atmospheric Chemistry and Physics Discussions

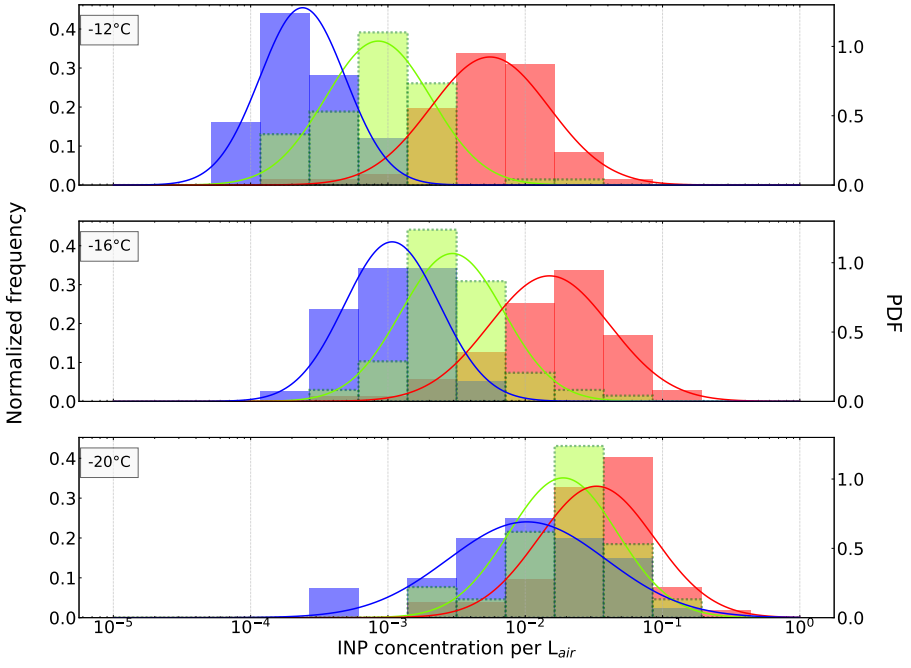

Figure 4. Normalized frequency distributions of N_{INP} at -12°C, -16°C and -20°C are shown as histograms, togehter with corresponding log-normal fits. The different colors represent Fletcher (winter) type in blue, Cooper (summer) type in red and mix type in light green, as described in Section 3.2.

Table 2. Parameters of the INP parameterizations presented in this study. In addition, parameters for fits with a fixed slope are also provided for comparison purpose. The temperature ranges where the fittings were applied are also given.

Type	A	s	Temperature range of the fits
Mix	$1.365 \cdot 10^{-5}$	-0.354	$-24 \leq T \leq -7$
Summer (fixed slope)	$1.232 \cdot 10^{-4}$	-0.3	$-20 \leq T \leq -9$
Summer	$2.111 \cdot 10^{-4}$	-0.263	$-20 \leq T \leq -9$
Winter (fixed slope)	$7.553 \cdot 10^{-8}$	-0.6	$-22 \leq T \leq -12$
Winter	$4.711 \cdot 10^{-7}$	-0.492	$-22 \leq T \leq -12$

two values for the slope originate from decades old, but are still widely used parametrizations by Fletcher (1962) and Cooper (1986), respectively. And, these are the two slopes that were at the basis of the categorization of different INP types (summer, winter and mix) used in this study (see Section 3.2). In Fig. 5, the parameterizations for the three different types are presented together with the maxima of the log-normal fits at each investigated temperature. The INP parameterizations are shown as solid lines, while the fixed slope fits are shown in dashed lines. Parameterizations from Cooper (1986), Fletcher (1962) and Li et al. (2022) were also plotted for comparison. All parameterizations in this study predict INP concentration up to three orders of magnitude lower than Cooper (1986) and Fletcher (1962). The parameterization from Li et al. (2022) compares very well with

https://doi.org/10.5194/acp-2022-761
Preprint. Discussion started: 17 November 2022


Atmospheric Chemistry and Physics Discussions

the parameterization suggested for the mix type in our study, with both sharing a very similar slope and the latter showing a concentration of only a factor of ≈ 3 lower. This is not surprising, as the parameterization by Li et al. (2022) was derived from measurements taking place in October and November 2019 and in March and April 2020, but further south on Svalbard. These months largely overlap with those that were found to be dominated by the mix type in our study (November) or not having a clearly dominating type (April and May), which clearly highlights the need to carry out long term measurements as done in the present paper in order to get the right understanding of the dynamics and processes of environmental parameters i.e. INPs. An overview of the frequency distributions of N_{INP} at the investigated temperature range, along with the suggested INP parameterizations, are shown in Fig. 6. Median, 25th and 75th percentile of each distribution are shown in solid and dashed lines. As expected, it can be seen that N_{INP} distributions feature an increasing trend with lowering temperatures. In general, summer type distributions show a higher median compared to mix type, while distributions of the winter type show a lower median compared to the mix type. This is consistent with what is shown in Fig. 4.

As described in Section 3.2, winter, summer and mix type show different fractions of occurrence throughout the year, varying depending on the month, but with summer and winter type dominating summer and winter months, respectively. In order to strategically implement the parameterizations from this study into climate and cloud-resolving models, the authors propose the following strongly simplified scheme:

- winter type, to be used during 60% ot the time from December to March, and 30% of the time in April, May and November:
  $N_{INP}(T) = 4.711 \cdot 10^{-7} \cdot e^{-0.492 \cdot T}$
- summer type, to be used during 60% of the time from June to October, and 30% of the time in April, May and November:
  $N_{INP}(T) = 2.111 \cdot 10^{-4} \cdot e^{-0.263 \cdot T}$
- mix type, to be used during 40% of the time throughout the year:
  $N_{INP}(T) = 1.365 \cdot 10^{-5} \cdot e^{-0.354 \cdot T}$

This is only a rough representation, and if favored, more highly resolved monthly values can be taken from Fig. 3. Overall, these result clearly show that differing parameterizations, depending on the the time of year, are needed to describe INPs in the Arctic. However, three different base cases, as those derived above, may suffice.

3.4 Bio-ratio and thermally-treated samples

Thermal treatment of the samples showed that the ice activity for most of the samples was reduced after heating for 1h at $85°C$ or $90°C$. The bio-ratio, which is used as a proxy for the fraction of biological INPs in each sample, was evaluated by using equation 5, as described in Section 2.2.7. A time series of the bio-ratio at $-12°C$, $-16°C$ and $-20°C$ is shown in Fig 7. A seasonal cycle is again observed at $-12°C$ and $-16°C$. In general, a higher fraction of biological INPs was found in samples collected during the snow-free months than during months with a snow-cover. It is also worth mentioning that even in snow-covered months, at $-12°C$, a bio-ratio of 0.75 or higher can be reached. At $-16°C$, the bio-ratios in both snow-free and

https://doi.org/10.5194/acp-2022-761
Preprint. Discussion started: 17 November 2022

Atmospheric Chemistry and Physics Discussions

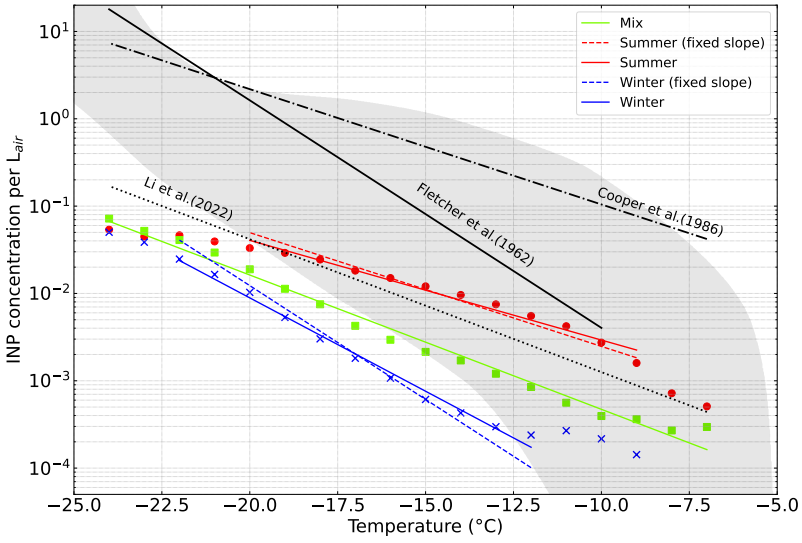

Figure 5. The INP parameterizations for summer, winter and mix type are shown as solid lines in red, blue and light green respectively. Maxima of the log-normal fits are also shown as dots with the respective colors. For comparison the fixed slope fits (cf. Section 3.3) are given as dashed lines of the respective type color. For reference, also the parameterizations by Cooper (1986), Fletcher (1962) and Li et al. (2022) are shown (black lines). Also for reference, the typical range of mid-latitude INP concentration according to Petters and Wright (2015) is shown as gray-shaded area.

snow-covered months are generally lower than at -12°C. At -20°C, not enough data points exist to provide an insight on the fraction of biological material.

Based on the categorization described before (i.e. winter, summer and mix type), the bio-ratio of samples separating into these types was examined as well. Box plots of these three types are shown in Fig. 8. Summer type in general shows the highest bio-ratio, while winter type shows the lowest. Mix type shows bio-ratio in between summer and winter type. This corroborates the interpretation in Section 3.2 that summer type is indeed dominated by biological INPs, with values often above 0.8, particularly above -15°C. Although the amount of background INPs cannot be directly interpreted through the bio-ratio plot, the relatively low amount of biological INPs in the winter type (compared with summer and mix type) indicates that roughly at least half of all INPs during that period were comprised of non-proteinaceous biological material. The atmospherically most abundant non-biological INPs are mineral dust particles. And as local Arctic sources are sparse in winter, due to the surface being covered in snow and ice, it is likely that the observed background INPs originate from long-range transport. All three types feature a decreasing bio-ratio with decreasing temperature, indicating that an increasing fraction of all INPs is contributed by background mineral dust towards lower temperatures. This is in line with the observation presented in Fig. 4, where the distributions of the three types converged at lower temperatures.

https://doi.org/10.5194/acp-2022-761
Preprint. Discussion started: 17 November 2022

Atmospheric Chemistry and Physics Discussions

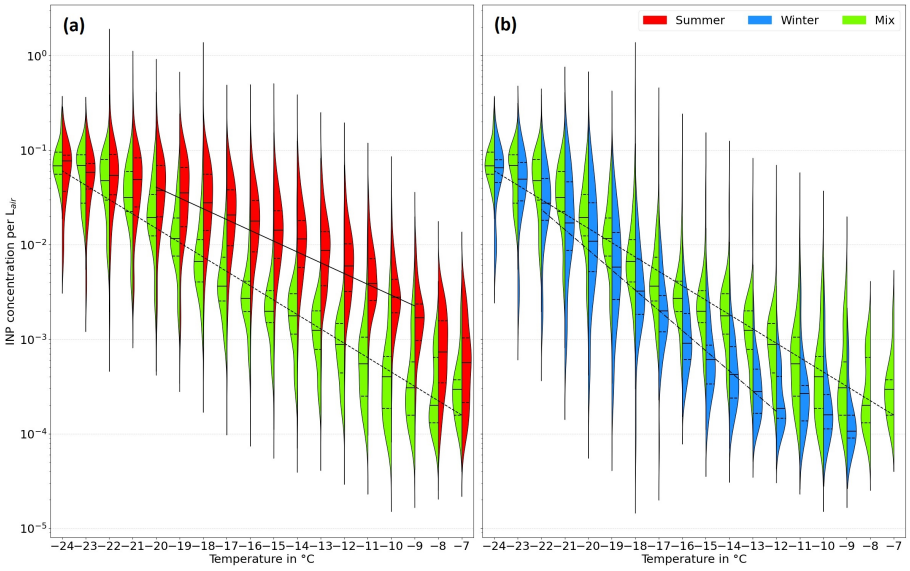

Figure 6. Violin plots of the $N_{INP}(T)$ frequency distribution from -7°C to -24°C, given in the typical color used for the corresponding types (panel a) summer type; panel b) winter type; both panels: mix type, shown in both panels for reference). For the distributions, solid horizontal lines show the median and dashed horizontal lines show the 25th and 75th percentile, respectively. The parameterizations suggested in this study are also plotted as solid black line (summer) in the left panel, and dash-dot black line (winter) in the right panel, and as dashed black line (mix) in both panels.

3.5 Case study

As seen in Fig. 1, N_{INP} in April 2020 was noticeably higher compared to the same month in 2019. To further investigate the cause of the differences, 5-day back-trajectories were used to determine the origin of the sampled air masses. In Fig. 9, examples are given for one filter collected in 2019 and one collected in 2020. Trajectories arriving at 50m are shown for locations where they were at heights below 250m (in red color). The trajectories are overlaid on the sea ice concentration map for the sampling period of the filters, which were sampled for 3.5 days prior to 1 April 2019 and 10 April 2020, respectively. Maps for all other filters collected in April 2019 and 2020 can be found in Fig. A7 and A8. The altitude threshold of 250 m was applied in order to locate potential source regions within the planetary boundary layer. It can be seen in Fig. 9 that for both filters the air masses arriving at VRS were only below 250 m in proximity to coastal areas of Greenland. Near the coast, both local marine and terrestrial sources can potentially contribute to the INP population.

The same 5-day back-trajectories were used further: To quantitatively investigate the difference of INP sources between April 2019 and 2020, the amount of time of trajectories spent above different surface types at altitudes below 250 m was evaluated for each sample collected during the two months and expressed in frequency in Fig. 10. The surface was categorized into the following types: terrestrial, open sea, sea ice concentration ($< 50\%$), sea ice concentration ($50 - 75\%$), sea ice concentration ($75 - 90\%$) and sea ice concentration ($90 - 100\%$). In both years sea ice with concentrations above 90% contributed the most

https://doi.org/10.5194/acp-2022-761
Preprint. Discussion started: 17 November 2022

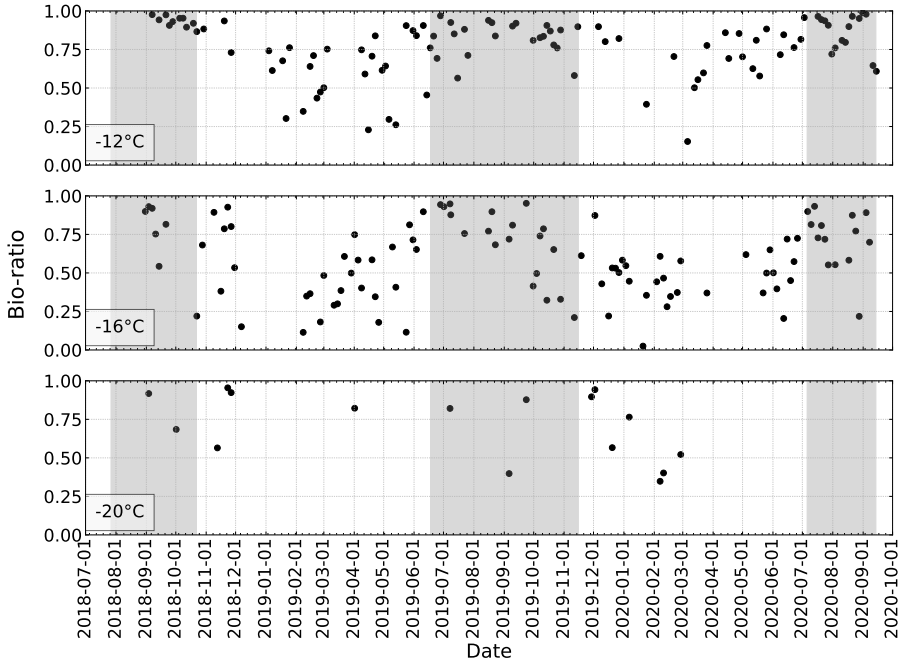

Figure 7. Times series of the bio-ratio at −12°C, −16°C and −20°C. The gray area indicates the time period with a snow depth below 0.8m.

to the air masses sampled for most of the filters, with some occasions when terrestrial surfaces and sea ice with lower concentration played a larger role. Values for these frequencies are shown in Table A3 and A4, respectively. This back-trajectory analysis shows no obvious difference in the air mass history between the two years. Satellite remote sensing products show that along the coastal areas in the investigated region, patches of low sea ice concentration and low snow cover exist. However, a more small-scale attribution of the air mass to these possible marine or terrestrial source regions is not meaningful when the accuracy of the back-trajectories and the satellite products is considered.

Further efforts were made by investigating the relation between the INP concentration and a broad range of available meteorological parameters, as mentioned in Section 2.2.8 and shown in Fig. 11. The values shown in the time series in Fig. 11 were averaged over the sampling period of each filter, and the right hand panels show a box plot each for all data points in 2019 and 2020. No significant dependence of INP concentration on meteorological parameters was observed in these two years. This can also be seen in the correlation plots in Fig. A9 and A10. Neither was there a difference between the two years which could meaningfully explain the difference in INP concentrations. Nevertheless, we highlight the following observations: the snow depth in 2020 was constantly above that in 2019, but they were, however, above 1 m at all times; maximum and mean wind speed and the surface temperature were all higher in the second half of the month in 2020 compared to in 2019. However, INP concentrations were elevated throughout all of April 2020. These higher values in the second half of April 2020 likely were connected to a warm air mass intrusion as observed on the research vessel Polarstern (Dada et al., 2022), which was roughly located at 84.6° N, 14° E, about 800 km north-east of VRS. This intrusion observed at Polarstern from April 14 to 16 likely

https://doi.org/10.5194/acp-2022-761
Preprint. Discussion started: 17 November 2022

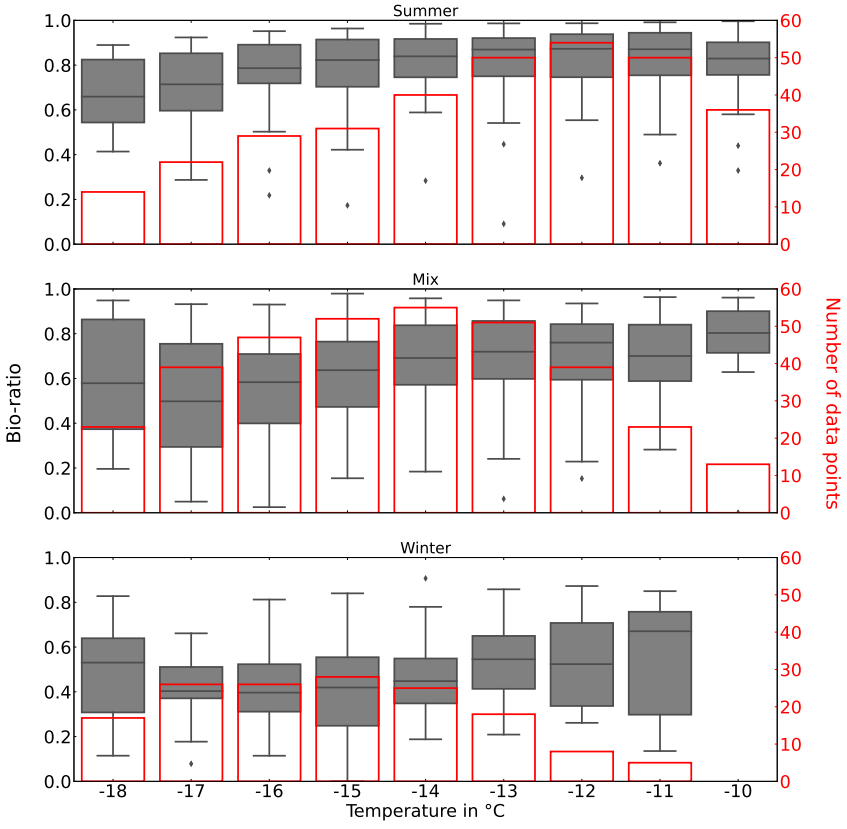

Figure 8. Box plots of the bio-ratio for summer, winter and mix type from −10°C to −18°C. Bar plots (in red) show the number of data points at each temperature.

connected to the higher temperatures and wind speeds observed at VRS in the second half of April. But again, this cannot explain the elevated INP concentrations observed throughout April 2020.

In a further effort, we examined if the increased INP concentrations in April 2020 correlated with the frequency of occurrence of ice in clouds, for which we obtained the CIF (Cloud Ice Frequency) from satellite data. In Fig. 12, temperature dependent CIFs for the 75-85° latitude band are shown for the months of April for altogether 11 years, from 2010 to 2020, together with an average curve for the years 2010-2018. For temperatures above −20°C, CIF for 2020 was above CIF for 2019 as well as above the average from 2010-2018. Figure 13 shows, that the effect of higher CIF in 2020 was indeed present in all of the latitudinal band above 80°, and particularly pronounced in Northern Greenland. Therefore, the higher INP concentrations observed at

https://doi.org/10.5194/acp-2022-761
Preprint. Discussion started: 17 November 2022

Atmospheric Chemistry and Physics Discussions

the surface may have caused a larger cloud ice content, which, in turn, may have influenced cloud radiative properties and precipitation formation and in turn cloud lifetime, resulting in an influence on surface temperatures. Also the increasing snow depth during April 2020 may result from stronger precipitation formation. While this is all speculative, the observed higher CIF in 2020 is clearly in line with the observed higher INP concentrations.

Overall, INP concentrations show no correlation between examined surface types and meteorological parameters. Efforts of correlating the INP concentration in the Arctic with aerosol physical properties such as aerosol concentration, fluorescent particle concentration and particle surface concentration were made in connection with a recent study by Li et al. (2022), in which also no relationship between INP concentrations and the above-mentioned parameters was found. This altogether illustrates the difficulties in predicting INP concentrations based on either INP sources or on meteorological parameters or on aerosol properties. Instead, as already also argued in Li et al. (2022), simple parameterizations, yielding temperature dependent INP concentrations, seem beneficial, with the constraint that these may differ by season, as the ones derived in this study.

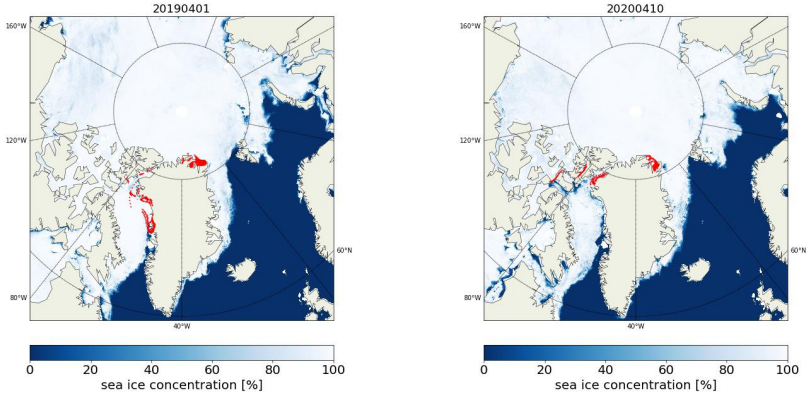

Figure 9. Shown in red are 5-day back-trajectories (50 m a.g.l. arrival height at VRS) for times when they were below 250m. The two panels correspond to sampling times of two filters, for which the sampling end dates were 1 April 2019 and 10 April 2020. Averaged sea ice concentrations during the sampling periods are also presented.

4 Summary and conclusions

Results from two-year-long INP measurements at Villum Research Station located in Northern Greenland have been presented in this study. Filter samples were collected on a half-weekly basis from July 2018 to September 2020. Off-line INP droplet freezing arrays were used to analyze the INP concentration, $N_{INP}(T)$, in the temperature range relevant for mixed-phase clouds. A seasonal cycle of N_{INP} was observed at higher temperatures, exemplary presented at -12°C and -16°C. Snow-free months featured clearly higher N_{INP} compared to months when the surface was snow-covered. This finding aligns with previous literature, such as Šantl Temkiv et al. (2019), Wex et al. (2019) and Creamean et al. (2018), describing higher INP concentrations

https://doi.org/10.5194/acp-2022-761
Preprint. Discussion started: 17 November 2022

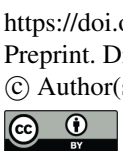

Atmospheric Chemistry and Physics Discussions

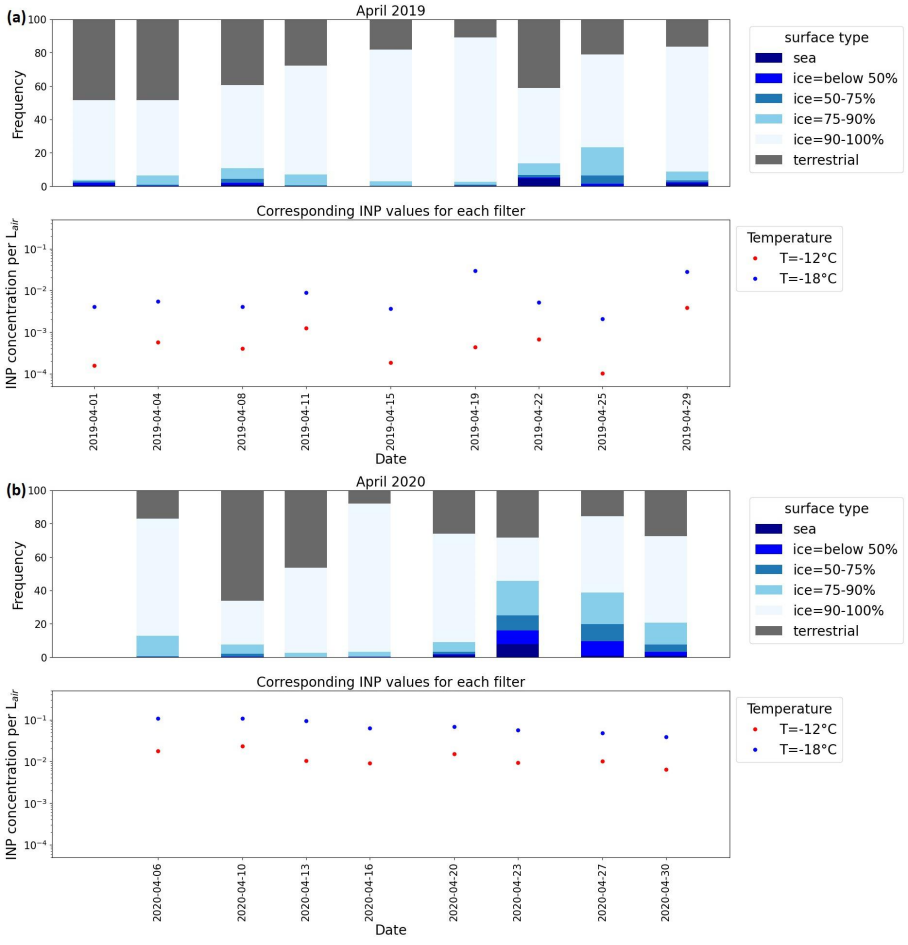

Figure 10. Frequency of the occurrence of different surface types below the trajectory for the sampling period of each filter collected in April 2019 (**a**; upper panel) and April 2020 (**b**; upper panel) are shown as stacked bar plots. Their corresponding INP concentration at -12°C and -18°C are shown in lower panels of (**a**) and (**b**) as reference. Data points are drawn at the end date of the sampling period of each of the 3.5 d filters.

during summer, compared to winter. Heating tests were performed in order to assess the fraction of proteinaceous, biological INPs in relation to the total amount of INPs (referred to as bio-ratio). A seasonal cycle was again observed for the bio-ratio at temperatures above -16°C. Nonetheless, even during months with surface snow-cover, bio-ratios at -12°C can be as high as 0.75 and sometimes even larger. Still, the higher bio-ratio in the months without snow-cover shows, that an annual cycle of N_{INP} mostly occurs due to the seasonality of biological sources throughout the year. The whole data-set was categorized based on the slope of the respective INP spectra, resulting in three types of spectra, namely summer, winter, and mix type. For these three types, the frequency distribution of N_{INP} was derived and fitted with log-normal distributions for different temperatures. At higher temperatures (e.g. -12°C) the maxima of the fitted distributions are clearly different from each other, while with

https://doi.org/10.5194/acp-2022-761
Preprint. Discussion started: 17 November 2022


Atmospheric Chemistry and Physics Discussions

decreasing temperature the differences between the distributions become less and less pronounced. This shows that at high temperatures distinct INP populations with different ice nucleation efficiencies are present, while at low temperatures only an almost uniform INP population seems to exist. This, together with the finding that the bio-ratio shows a decreasing amount of biological INPs with decreasing temperature is interpreted as follows: Highly ice active biological INPs are the cause for high INP concentrations at high temperatures (roughly -16°C and above). These highly efficient INPs occur additionally to a more generally present and less efficient background INP population. With decreasing temperature the biolgocial INPs become less prominent, until they blend with the background INP population at the lower temperatures (-20°C and below). A temperature dependent INP parameterization based on the mean concentrations of the temperature dependent PDF was derived for each of the aforementioned types (winter, summer and mix). While the summer type INP spectra occured during 60% of all times in the summer months, and the winter type during 60% of all times during the winter months, the mix type occured 40% of all times year-round, and April, May and November were transition months. With this information, these parameterizations can be easily implemented into climate and cloud-resolving models, because they only depend on temperature and the month of the year in order to deliver a prediction of $N_{INP}(T)$ in the high Arctic throughout the year. This will improve the description of the annual cycle of INP concentrations as observed in the Arctic for modelling purposes.

A case study investigating possible causes for significant differences in N_{INP} found between April 2019 and 2020 was carried out. Back-trajectories indicate that the sampled air masses mainly originated from coastal regions of Greenland in both years. Therefore, both local terrestrial and marine sources could potentially contribute to the collected INPs. INP concentration shows no dependency on different surface types and meteorological parameters in these two periods, and no parameter was found which was clearly different in April 2019 and April 2020. However, examining satellite data, we found a higher cloud ice fraction for the year with higher INP concentrations, suggesting a possible link between INP concentration and ice in clouds. Altogether the results of our investigations indicate the complexity of predicting Arctic INP and their effects on clouds. It further emphasizes the need for suitable models from the LES to global scales, and the importance of using appropriate, e.g. solely temperature based parameterizations therein.

https://doi.org/10.5194/acp-2022-761
Preprint. Discussion started: 17 November 2022

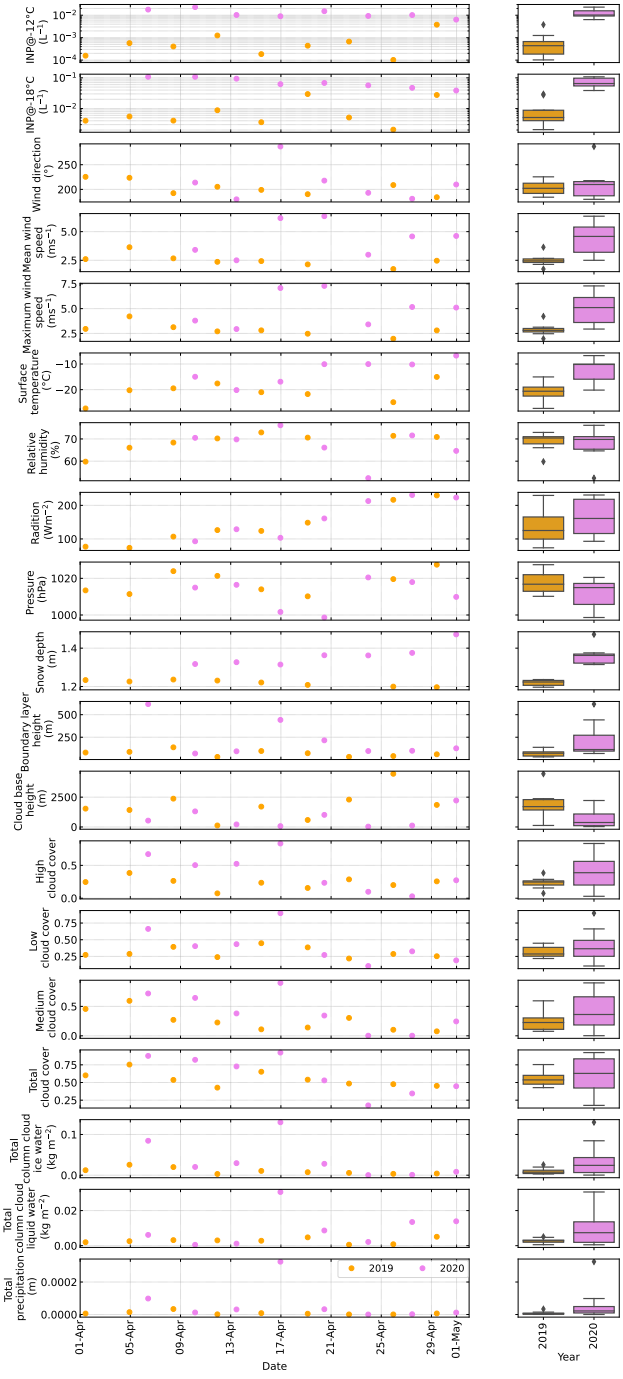

Figure 11. Filter-wise average of investigated meteorological parameters as well as the INP concentration at −12°C and −18°C, in April 2019 (orange) and 2020 (purple) are shown in time series (left). Corresponding box plots of all data points in the April of the respective year are shown on the right hand panel.

https://doi.org/10.5194/acp-2022-761
Preprint. Discussion started: 17 November 2022

Atmospheric Chemistry and Physics Discussions

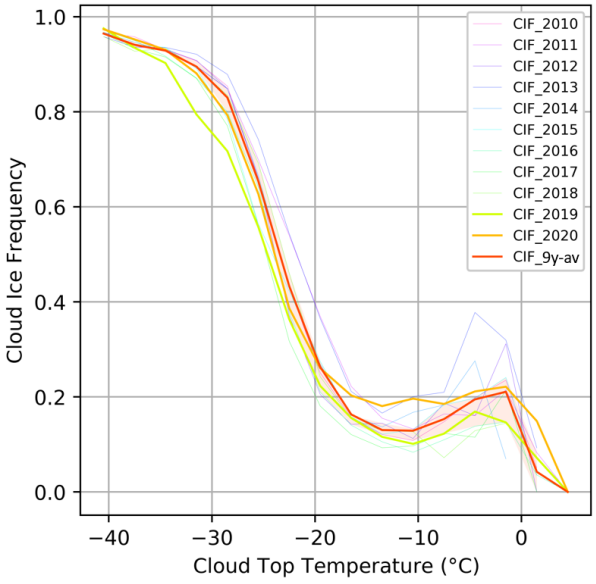

Figure 12. Temperature dependent CIFs at the latitude band between 75N and 85N for the years 2010 to 2020, and the average for 2010-2018 (with the shaded area covering the 25th to 75th percentile).

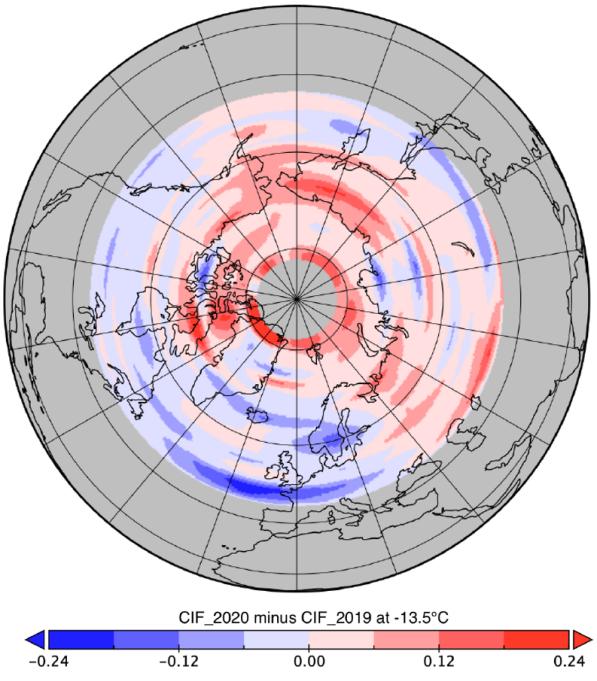

Figure 13. CIF during April 2020 minus CIF during April 2019 at a cloud top temperature of -13.5°C (only data above 45° N are shown).

https://doi.org/10.5194/acp-2022-761
Preprint. Discussion started: 17 November 2022

Atmospheric Chemistry and Physics Discussions

Appendix A

A1 Merging procedure of INP spectra from LINA and INDA

As mentioned in the main text, all spectra of untreated samples shown in this study are merged from the individual LINA and INDA spectra of the respective sample. The procedure to achieve the merged spectra is described in the following paragraphs. The first two steps of the merging procedure are associated with data quality assurance: Due to the temperature calibration functions for LINA and INDA, the temperatures at which the $f_{ice}(T)$ were measured differ for the two setups. Details on the calibration of LINA and INDA can be found in the SI of Hartmann et al. (2021). To obtain unified temperatures for all data sets, in a first step, a linear interpolation was done for all measured frozen fraction spectra of LINA and INDA. This resulted in $f_{ice}(T)$ for every tenth of a degree. As the second step of the merging procedure, the spectra of LINA and INDA were truncated, i.e., $f_{ice}(T)$ corresponding to the first three and last two frozen droplets were deleted, i.e. for LINA, $\frac{3}{90} < f_{ice}(T) < \frac{89}{90}$; while for INDA, $\frac{3}{48} < f_{ice}(T) \leq \frac{46}{48}$. This was done due to the large statistical uncertainty of this data. As the next step of the merging procedure, the area between the LINA and INDA spectra in the overlap temperature range was quantified as the sum of the absolute difference of INP number concentration (per volume of water) $N_{INP,water}$ at each temperature, divided by the temperature range of the overlap region. An example is shown in Fig. A1a. Those spectra that had an area larger than the 95^{th} percentile of the whole data-set were discarded from further analysis. The remaining spectra fulfilled the authors' standards for data quality and were then converted into atmospheric INP number concentration $N_{INP,air}$ (see Fig. A1b) and merged as described as follows: A merging weighting factor F(T) was calculated for both LINA and INDA spectra based on their corresponding frozen fraction. The idea behind F(T) is to account for the fact that a high f_{ice} value, and the N_{INP} value derived from it, is statistically more certain than a low one. When the spectra are merged, the statistically more certain values at a given T should therefore be weighted more strongly. F(T) is calculated as follows:

$$F_{\mathrm{LINA}}(T) = \frac{f_{\mathrm{ice,LINA}}(T)}{f_{\mathrm{ice,LINA}}(T) + f_{\mathrm{ice,INDA}}(T)} \tag{A1}$$

and

$$F_{\mathrm{INDA}}(T) = \frac{f_{\mathrm{ice,INDA}}(T)}{f_{\mathrm{ice,LINA}}(T) + f_{\mathrm{ice,INDA}}(T)} \tag{A2}$$

By using the merging weighting factors above, the INP number concentration of the merged spectrum ($N_{INP,merge}$) in the overlap region is then calculated as

$$N_{\mathrm{INP,merge}}(T) = N_{\mathrm{INP,LINA}}(T) \cdot F_{\mathrm{LINA}}(T) + N_{\mathrm{INP,INDA}}(T) \cdot F_{\mathrm{INDA}}(T) \tag{A3}$$

where $N_{INP,LINA}(T)$ is the INP number concentration of LINA spectra in the overlap region, while $N_{INP,INDA}(T)$ is the INP number concentration of INDA spectra in the overlap region. Along with the non-overlap region, a full INP spectrum (i.e. merged region, non-overlap INDA region, non-overlap LINA region) is derived (see Fig. A1c). For simplicity, the atmospheric INP number concentration of the full spectrum is denoted as N_{INP} in this study. It is also worth to point out that by merging INP spectra of LINA and INDA, it is possible that in rare cases, as temperature decreases, the INP number concentration of the full spectrum decreases.

https://doi.org/10.5194/acp-2022-761
Preprint. Discussion started: 17 November 2022

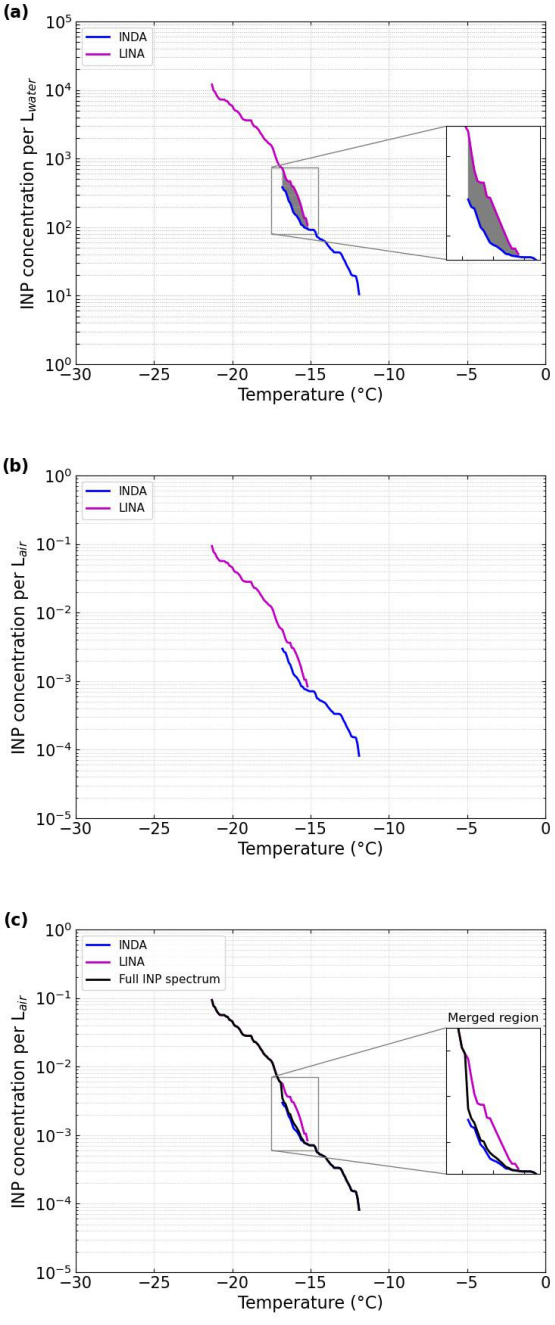

Figure A1. A schematic sketch of the merging procedures performed in this study. a) After interpolation and truncation of both LINA (in purple) and INDA (in blue) spectra, the consistency of the spectra was evaluated by quantifying the area (gray color) between the two spectra. Note that the INP concentration shown here is per liter of water. Spectra showed area large than 95^{th} percentile of the whole data-set were discarded. b) INP concentration per liter of air of the remaining samples was calculated. c) Merging was taken place followed the calculations mentioned in text. The INP concentration N_{INP} of the full spectrum (in black) was then used for data interpretation.

https://doi.org/10.5194/acp-2022-761
Preprint. Discussion started: 17 November 2022

Atmospheric Chemistry and Physics Discussions

A2 INP spectra characterization

In a further step, the fraction of heat-labile INPs, i.e., the bio-ratio (see Section 3.4), in relation to the classification described in Section 3.2 was also investigated. The result is shown in Fig. A2. Indeed, at the depicted temperatures, for winter type samples, there are low bio-ratios of mostly only up to 50%, while summer type samples show high bio-ratios of mostly above 75%. The mix type samples are in between. This once more corroborates that the selected simple criteria to discriminate between the three different types of INP spectra are also in accordance with other INP properties which change over the year.

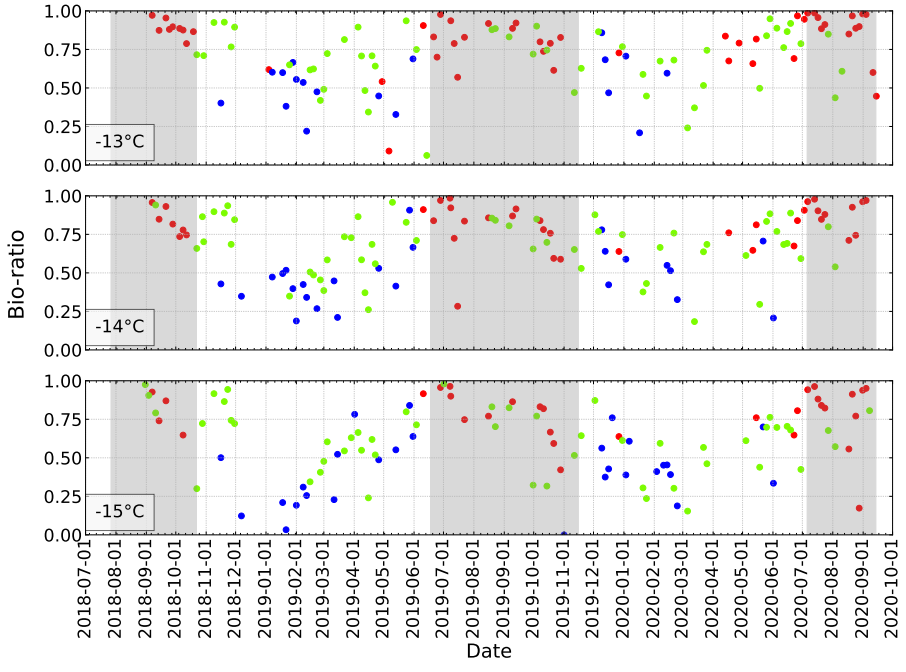

Figure A2. Time series of fractions of heat-labile INPs at three different temperatures, -13°C, -14°C and -15°C, with winter type data shown in blue, summer type data shown in red and mix type data shown in light green.

https://doi.org/10.5194/acp-2022-761
Preprint. Discussion started: 17 November 2022

Atmospheric Chemistry and Physics Discussions

A3 Sample summary

Table A1. Summary of the amount of filters analyzed. In total 181 filter samples were presented in this study.

Month	Year			Sum
	2018	2019	2020	
January	–	7	6	13
February	–	8	8	16
March	–	7	7	14
April	–	9	8	17
May	–	7	8	15
June	–	7	9	16
July	4	7	9	20
August	1	3	9	13
September	8	6	4	18
October	8	9	–	17
November	7	5	–	12
December	1	9	–	10

https://doi.org/10.5194/acp-2022-761
Preprint. Discussion started: 17 November 2022

Atmospheric Chemistry and Physics Discussions

Table A2. Summary of the amount of filters characterized as winter, mix and summer type.

Month	**Year**								
	2018			2019			2020		
	Winter	Mix	Summer	Winter	Mix	Summer	Winter	Mix	Summer
January	–	–	–	5	1	1	4	2	0
February	–	–	–	4	4	0	6	2	0
March	–	–	–	3	4	0	2	4	1
April	–	–	–	2	6	1	0	0	8
May	–	–	–	3	2	2	2	4	2
June	–	–	–	0	3	4	1	5	3
July	0	2	2	0	1	6	0	2	7
August	0	1	0	0	2	1	0	2	7
September	0	2	6	0	2	4	0	1	3
October	0	4	4	1	2	6	–	–	–
November	2	5	0	0	3	2	–	–	–
December	1	0	0	5	3	1	–	–	–

https://doi.org/10.5194/acp-2022-761
Preprint. Discussion started: 17 November 2022

Atmospheric Chemistry and Physics Discussions

A4 Instrumental uncertainties of LINA and INDA

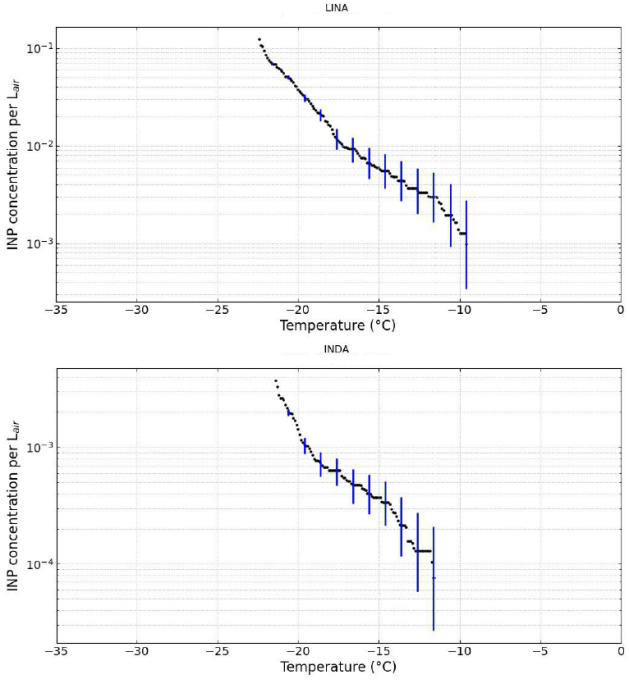

Figure A3. Example of INP spectra from two different filters with error bars in blue color showing the instrumental uncertainties of LINA (upper panel) and INDA (lower panel) in every 1°C step.

https://doi.org/10.5194/acp-2022-761
Preprint. Discussion started: 17 November 2022

Atmospheric Chemistry and Physics Discussions

A5 Overview of INP spectra

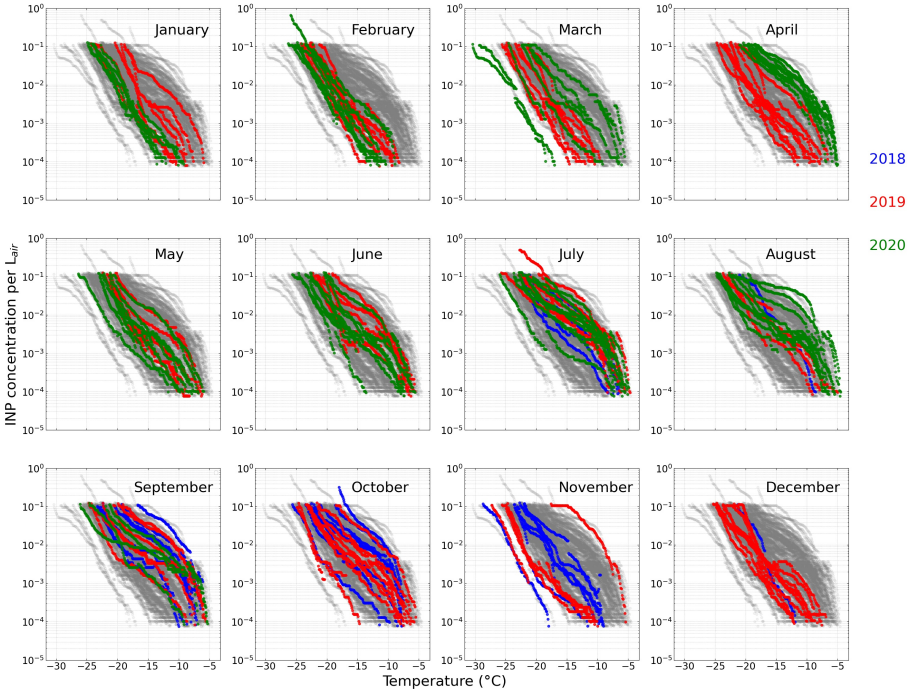

Figure A4. An overview of all INP spectra obtained in this study, color-coded by their corresponding year. Blue color shows samples collected in 2018, red color shows samples collected in 2019, green color shows samples collected in 2020, grey color shows all samples regardless of the collection months.

https://doi.org/10.5194/acp-2022-761
Preprint. Discussion started: 17 November 2022

Atmospheric Chemistry and Physics Discussions

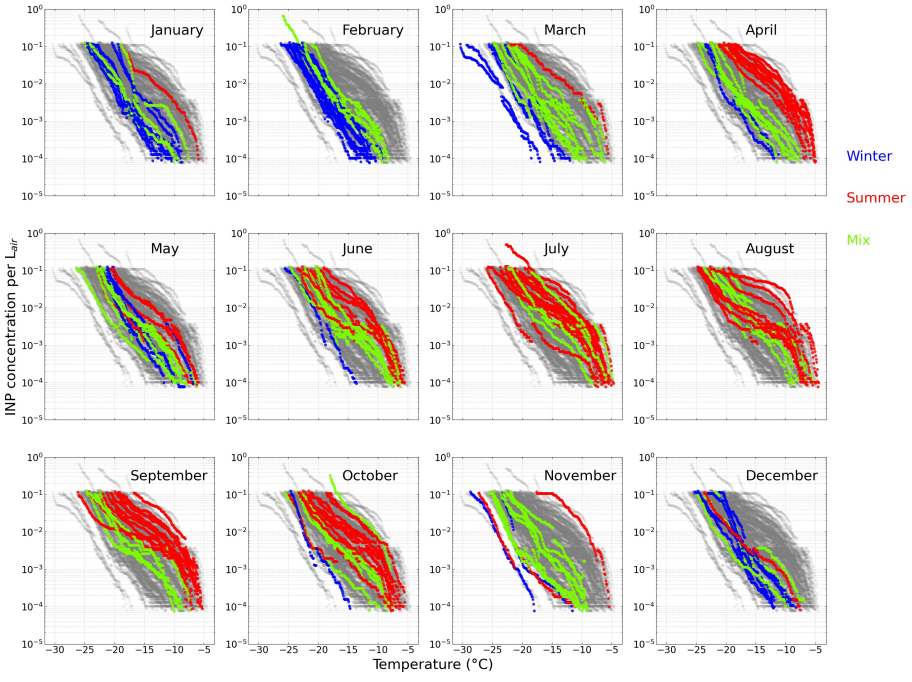

Figure A5. Similar figure as Fig. A4, color-coded by the types of categorization. Blue color shows samples characterized as winter type, red color shows samples characterized as summer type, light green show samples characterized as mix type, grey color shows all sampled filters regardless of their type.

https://doi.org/10.5194/acp-2022-761
Preprint. Discussion started: 17 November 2022

Atmospheric Chemistry and Physics Discussions

A6 Snow depth at Villum Research Station

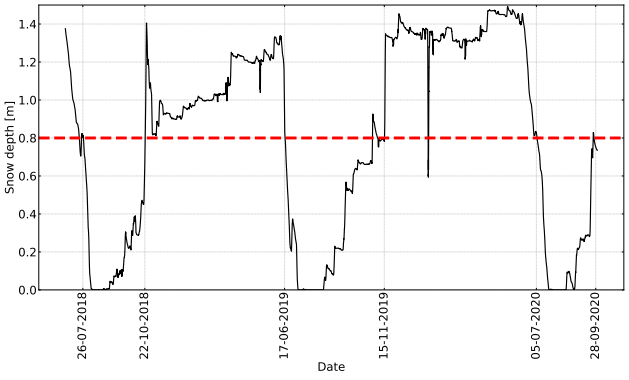

Figure A6. Snow depth measured at Villum Research Station. Dates shown on the x-axis in the figure specify the period when snow depth was below 0.8m.

https://doi.org/10.5194/acp-2022-761
Preprint. Discussion started: 17 November 2022

Atmospheric Chemistry and Physics Discussions

A7 Case study

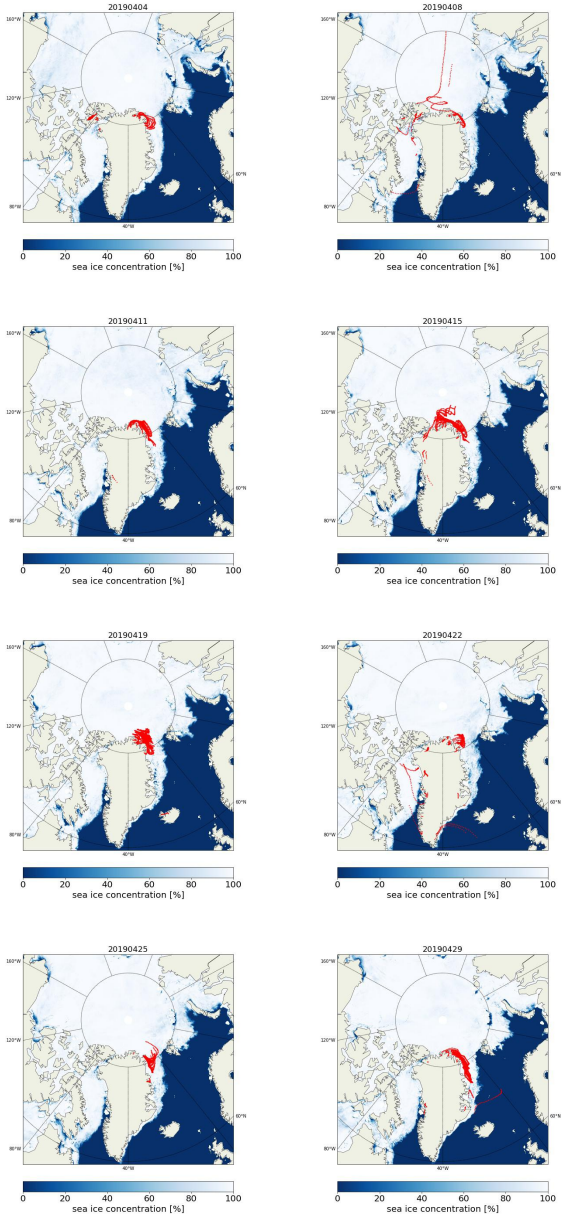

Figure A7. Each map shows trajectories and sea ice concentrations corresponding to an individual filter sample. All filters collected in April 2019 are shown. The sampling end date of the filters is shown on top of the maps. 5-day back-trajectories (arriving at VRS at a height of 50m) are indicated in red for locations where they were below 250m height. Average sea ice concentrations for the respective sampling periods are also shown.

https://doi.org/10.5194/acp-2022-761
Preprint. Discussion started: 17 November 2022

Atmospheric Chemistry and Physics Discussions

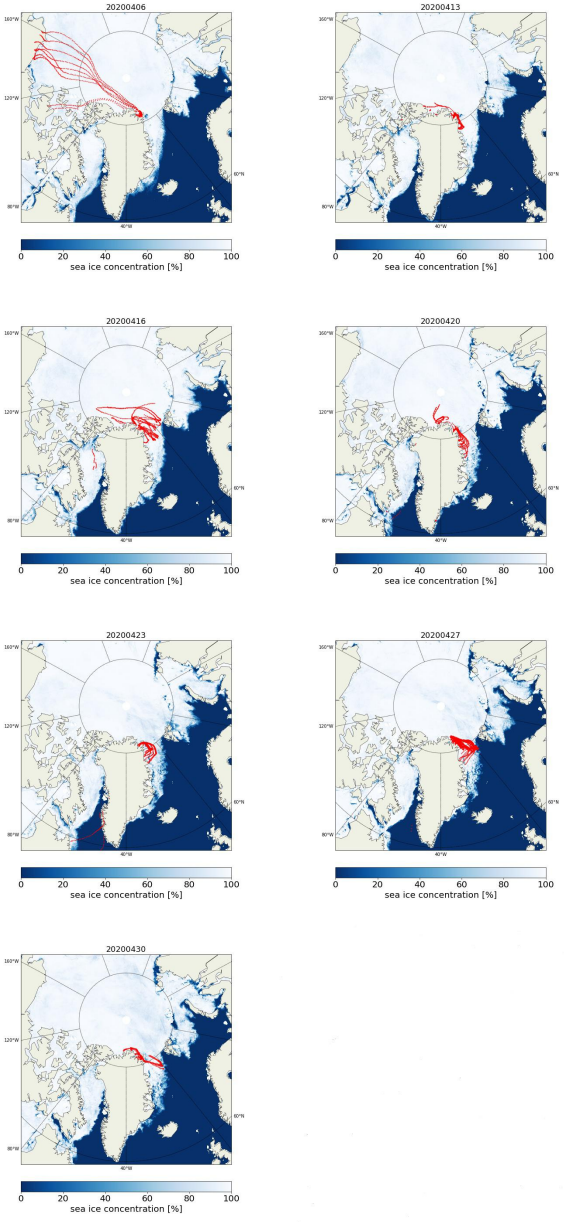

Figure A8. Each map shows trajectories and sea ice concentrations corresponding to an individual filter sample. All filters collected in April 2020 are shown. The sampling end date of the filters is shown on top of the maps. 5-day back-trajectories (arriving at VRS at a height of 50m) are indicated in red for locations where they were below 250m height. Average sea ice concentrations for the respective sampling periods are also shown.

https://doi.org/10.5194/acp-2022-761
Preprint. Discussion started: 17 November 2022

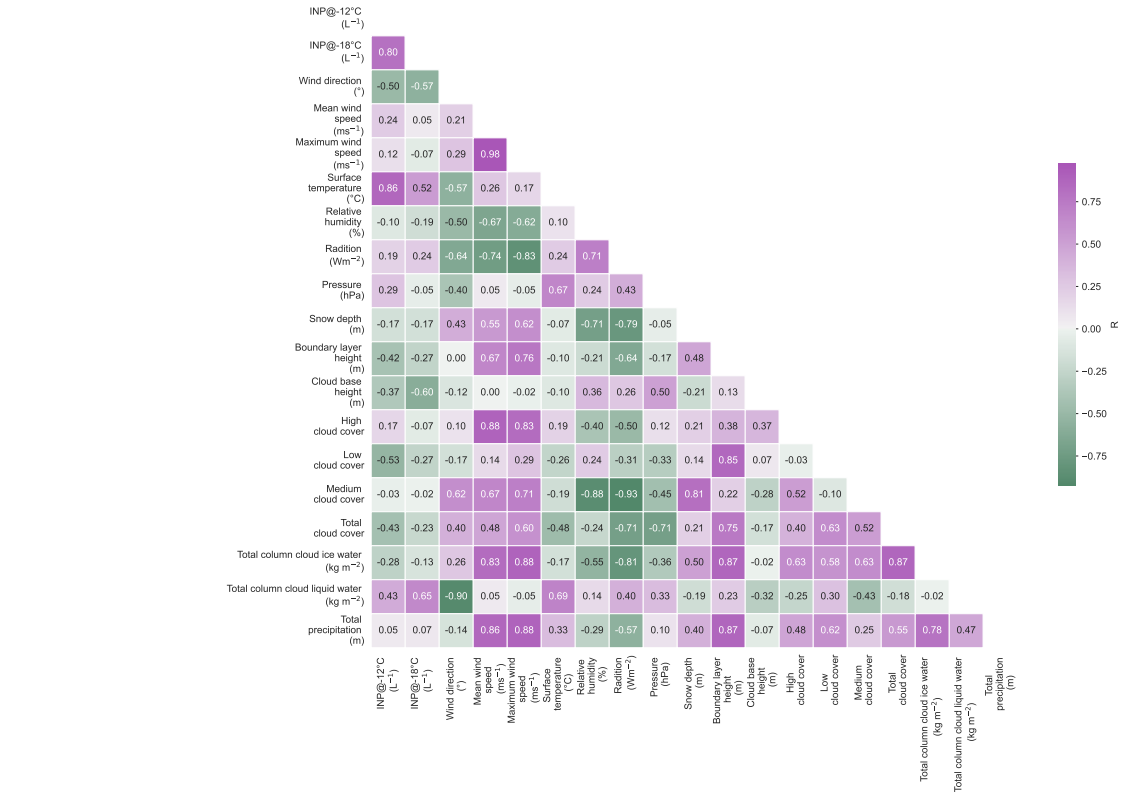

Figure A9. Correlation plot between N_{INP} at −12°C and −18°C and all examined meteorological parameters in April 2019. Value R shows the Spearman coefficient.

https://doi.org/10.5194/acp-2022-761
Preprint. Discussion started: 17 November 2022

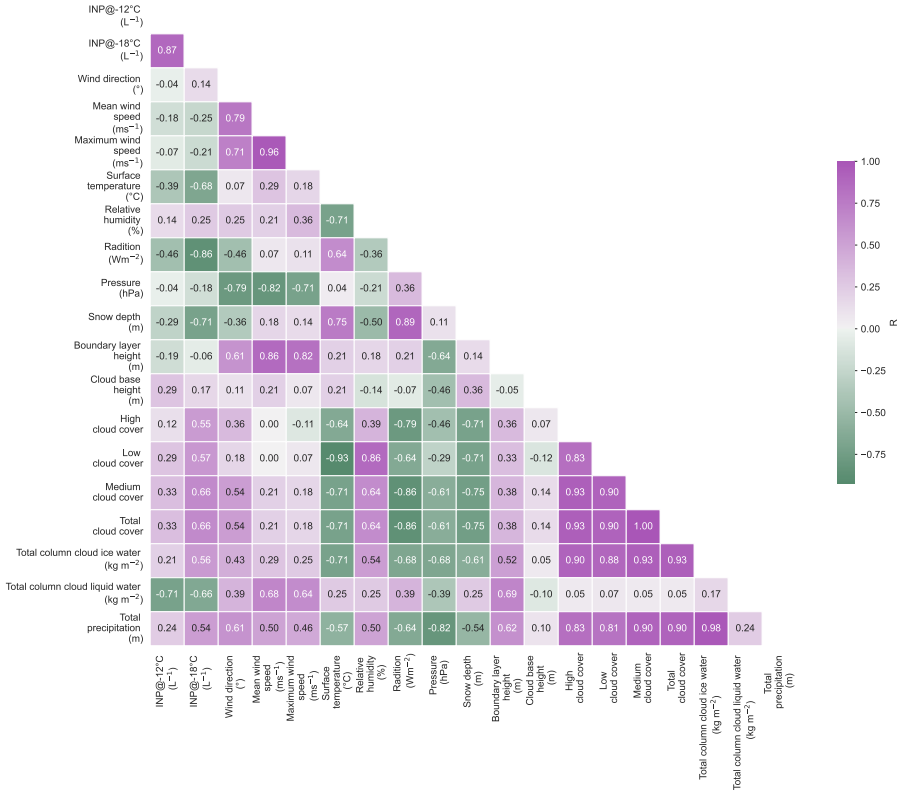

Figure A10. Correlation plot between N_{INP} at −12°C and −18°C and all examined meteorological parameters in April 2020. Value R shows the Spearman coefficient.

https://doi.org/10.5194/acp-2022-761
Preprint. Discussion started: 17 November 2022

Atmospheric Chemistry and Physics Discussions

Table A3. Summary of the frequency of surface types shown in Fig. 10(a). Values are expressed in %.

Surface type	Date								
	20190401	20190404	20190408	20190411	20190415	20190419	20190422	20190425	20190429
terrestrial	48.47	48.35	39.36	27.70	18.23	10.74	41.10	21.12	16.41
ice (90-100%)	47.65	45.19	49.86	65.29	78.85	86.71	45.13	55.45	74.82
ice (75-90%)	1.12	5.67	6.49	6.50	2.53	1.84	7.08	17.13	5.34
ice (50-75%)	0.82	0.66	2.21	0.42	0.34	0.42	1.47	4.90	1.18
ice (below 50%)	1.43	0.13	1.10	0.08	0.05	0.09	0.49	1.40	0.69
sea	0.51	0	0.97	0	0	0.19	4.72	0	1.57

Table A4. Summary of the frequency of surface types shown in Fig. 10(b). Values are expressed in %.

Surface type	Date							
	20200406	20200410	20200413	20200416	20200420	20200423	20200427	20200430
terrestrial	16.86	66.35	46.55	7.81	25.90	28.44	15.66	27.5
ice (90-100%)	70.32	26.09	50.96	89.06	65.04	25.74	45.67	51.92
ice (75-90%)	12.13	5.67	2.49	2.73	5.90	20.72	18.95	12.88
ice (50-75%)	0.69	1.51	0	0.20	1.58	9.14	10.12	4.42
ice (below 50%)	0	0.38	0	0.20	0.58	7.98	8.77	2.5
sea	0	0	0	0	1.01	7.98	0.82	0.77

https://doi.org/10.5194/acp-2022-761
Preprint. Discussion started: 17 November 2022

Atmospheric Chemistry and Physics Discussions

Data availability. INP data will be made publicly available at https://www.pangaea.de upon acceptance of the manuscript.

Author contributions. F.S. and H.W. conceptualized the study, H.S. and A.M. oversaw the sampling of filters at VRS, and K.S. did the INP measurements of the filter samples and analyzed the results. D.V. analyzed the satellite data. K.S., M.H., H.W. and F.S. advanced the overall analysis further. K.S. wrote the manuscript with support from all co-authors.

Competing interests. The authors declare that they have no conflict of interest.

Acknowledgements. We gratefully acknowledge the funding by the Deutsche Forschungsgemeinschaft (DFG, German Research Foundation) – Projektnummer 268020496 – TRR 172, within the Transregional Collaborative Research Center "ArctiC Amplification: Climate Relevant Atmospheric and SurfaCe Processes, and Feedback Mechanisms (AC)^3". The Villum Foundation is gratefully acknowledged for financing the Villum Research Station. The results contain modified Copernicus Climate Change Service information 2020. Neither the European Commission nor ECMWF is responsible for any use that may be made of the Copernicus information or data it contains. We thank Dominik Jammal and Johanna Seidel for their assistance of INP measurement. We also thank Martin Radenz for help running HYSPLIT model and providing the respective backward trajectories data files.

https://doi.org/10.5194/acp-2022-761
Preprint. Discussion started: 17 November 2022

Atmospheric Chemistry and Physics Discussions

References

Agresti, A. and Coull, B. A.: Approximate is Better than "Exact" for Interval Estimation of Binomial Proportions, The American Statistician, 52, 119–126, https://doi.org/10.1080/00031305.1998.10480550, 1998.

Augustin-Bauditz, S., Wex, H., Kanter, S., Ebert, M., Niedermeier, D., Stolz, F., Prager, A., and Stratmann, F.: The immersion mode ice nucleation behavior of mineral dusts: A comparison of different pure and surface modified dusts, Geophysical Research Letters, 41, https://doi.org/10.1002/2014gl061317, 2014.

Avery, M. A., Ryan, R. A., Getzewich, B. J., Vaughan, M. A., Winker, D. M., Hu, Y. X., Garnier, A., Pelon, J., and Verhappen, C. A.: CALIOP V4 cloud thermodynamic phase assignment and the impact of near-nadir viewing angles, Atmospheric Measurement Techniques, 13, 4539–4563, https://doi.org/10.5194/amt-13-4539-2020, 2020.

Bigg, E. and Leck, C.: Cloud-active particles over the central Arctic Ocean, Journal of Geophysical Research, 106, 32 155–32 166, https://doi.org/10.1029/1999jd901152, 2001.

Bigg, E. K.: Ice forming nuclei in the high Arctic, Tellus B, 48, 223–233, https://doi.org/10.3402/tellusb.v48i2.15888, 1996.

Boer, G., Morrison, H., Shupe, M. D., and Hildner, R.: Evidence of liquid dependent ice nucleation in high-latitude stratiform clouds from surface remote sensors, Geophysical Research Letters, 38, https://doi.org/10.1029/2010gl046016, 2011.

Borys, R. D.: Studies of ice nucleation by Arctic aerosol on AGASP-II, Journal of Atmospheric Chemistry, 9, 169–185, https://doi.org/10.1007/bf00052831, 1989.

Boucher, O., Randall, D., Artaxo, P., Bretherton, C., Feingold, G., Forster, P., Kerminen, V.-M., Kondo, Y., Liao, H., Lohmann, U., Rasch, P., Satheesh, S., Sherwood, S., Stevens, B., and Zhang, X.: Clouds and Aerosols, pp. 571–892, 2013.

Budke, C. and Koop, T.: BINARY: an optical freezing array for assessing temperature and time dependence of heterogeneous ice nucleation, Atmospheric Measurement Techniques, 8, 689–703, https://doi.org/10.5194/amt-8-689-2015, 2015.

Cohen, J., Screen, J., Furtado, J., Barlow, M., Whittleston, D., Coumou, D., Francis, J., Dethloff, K., Entekhabi, D., Overland, J., and Jones, J.: Recent Arctic amplification and extreme mid-latitude weather, Nature Geoscience, 7, 627–637, https://doi.org/10.1038/ngeo2234, 2014.

Cohen, J., Zhang, X., Francis, J., Jung, T., Kwok, R., Overland, J., Ballinger, T., Bhatt, U., Chen, H., Coumou, D., Feldstein, S., Gu, H., Handorf, D., Henderson, G., Ionita, M., Kretschmer, M., Laliberte, F., Lee, S., Linderholm, H., Maslowski, W., Peings, Y., Pfeiffer, K., Rigor, I., Semmler, T., Stroeve, J., Taylor, P., Vavrus, S., Vihma, T., Wang, S., Wendisch, M., Wu, Y., and Yoon, J.: Divergent consensuses on Arctic amplification influence on midlatitude severe winter weather, Nature Climate Change, 10, 20–29, https://doi.org/10.1038/s41558-019-0662-y, 2020.

Coluzza, I., Creamean, J., Rossi, M., Wex, H., Alpert, P., Bianco, V., Boose, Y., Dellago, C., Felgitsch, L., Fröhlich-Nowoisky, J., Herrmann, H., Jungblut, S., Kanji, Z., Menzl, G., Moffett, B., Moritz, C., Mutzel (formerly Heinold), A., Pöschl, U., Schauperl, M., and Schmale, D.: Perspectives on the Future of Ice Nucleation Research: Research Needs and Unanswered Questions Identified from Two International Workshops, Atmosphere, 8, 138, https://doi.org/10.3390/atmos8080138, 2017.

Conen, F., Morris, C. E., Leifeld, J., Yakutin, M. V., and Alewell, C.: Biological residues define the ice nucleation properties of soil dust, Atmospheric Chemistry and Physics, 11, 9643–9648, https://doi.org/10.5194/acp-11-9643-2011, 2011.

Conen, F., Rodríguez, S., Hülin, C., Henne, S., Herrmann, E., Bukowiecki, N., and Alewell, C.: Atmospheric ice nuclei at the high-altitude observatory Jungfraujoch, Switzerland, Tellus B: Chemical and Physical Meteorology, 67, 25 014, https://doi.org/10.3402/tellusb.v67.25014, 2015.

https://doi.org/10.5194/acp-2022-761
Preprint. Discussion started: 17 November 2022

Atmospheric Chemistry and Physics Discussions

Conen, F., Stopelli, E., and Zimmermann, L.: Clues that decaying leaves enrich Arctic air with ice nucleating particles, Atmospheric Environment, 129, https://doi.org/10.1016/j.atmosenv.2016.01.027, 2016.

Cooper, E. J.: Warmer Shorter Winters Disrupt Arctic Terrestrial Ecosystems, Annual Review of Ecology, Evolution, and Systematics, 45, 271–295, https://doi.org/10.1146/annurev-ecolsys-120213-091620, 2014.

Cooper, W. A.: Ice Initiation in Natural Clouds, Meteorological Monographs, 21, 29–32, https://doi.org/10.1175/0065-9401-21.43.29, 1986.

Creamean, J., Cross, J., Pickart, R., McRaven, L., Lin, P., Pacini, A., Hanlon, R., Schmale, D., Ceniceros, J., Aydell, T., Colombi, N., Bolger, E., and DeMott, P.: Ice Nucleating Particles Carried From Below a Phytoplankton Bloom to the Arctic Atmosphere, Geophysical Research Letters, 46, https://doi.org/10.1029/2019gl083039, 2019.

Creamean, J., Hill, T., DeMott, P., Uetake, J., Kreidenweis, S., and Douglas, T.: Thawing permafrost: an overlooked source of seeds for Arctic cloud formation, Environmental Research Letters, 15, https://doi.org/10.1088/1748-9326/ab87d3, 2020.

Creamean, J. M., Kirpes, R. M., Pratt, K. A., Spada, N. J., Maahn, M., de Boer, G., Schnell, R. C., and China, S.: Marine and terrestrial influences on ice nucleating particles during continuous springtime measurements in an Arctic oilfield location, Atmospheric Chemistry and Physics, 18, 18 023–18 042, https://doi.org/10.5194/acp-18-18023-2018, 2018.

Creamean, J. M., Barry, K., Hill, T. C. J., Hume, C., DeMott, P. J., Shupe, M. D., Dahlke, S., Willmes, S., Schmale, J., Beck, I., Hoppe, C. J. M., Fong, A., Chamberlain, E., Bowman, J., Scharien, R., and Persson, O.: Annual cycle observations of aerosols capable of ice formation in central Arctic clouds, Nature Communications, 13, https://doi.org/10.1038/s41467-022-31182-x, 2022.

Dada, L., Angot, H., Beck, I., Baccarini, A., Quelever, L. L. J., Boyer, M., Laurila, T., Brasseur, Z., Jozef, G., de Boer, G., Shupe, M. D., Henning, S., Bucci, S., Dutsch, M., Stohl, A., Petaja, T., Daellenbach, K. R., Jokinen, T., and Schmale, J.: A central arctic extreme aerosol event triggered by a warm air-mass intrusion, Nature Communications, 13, https://doi.org/10.1038/s41467-022-32872-2, 2022.

DeMott, P., Brooks, S., Prenni, A., Kreidenweis, S., Sassen, K., Poellot, M., Rogers, D., and Baumgardner, D.: African Dust Aerosols as Atmospheric Ice Nuclei, Geophys. Res. Lett., 30, https://doi.org/10.1029/2003gl017410, 2003.

DeMott, P. J., Prenni, A. J., McMeeking, G. R., Sullivan, R. C., Petters, M. D., Tobo, Y., Niemand, M., Möhler, O., Snider, J. R., Wang, Z., and Kreidenweis, S. M.: Integrating laboratory and field data to quantify the immersion freezing ice nucleation activity of mineral dust particles, Atmospheric Chemistry and Physics, 15, 393–409, https://doi.org/10.5194/acp-15-393-2015, 2015.

DeMott, P. J., Hill, T. C. J., McCluskey, C. S., Prather, K. A., Collins, D. B., Sullivan, R. C., Ruppel, M. J., Mason, R. H., Irish, V. E., Lee, T., Hwang, C. Y., Rhee, T. S., Snider, J. R., McMeeking, G. R., Dhaniyala, S., Lewis, E. R., Wentzell, J. J. B., Abbatt, J., Lee, C., Sultana, C. M., Ault, A. P., Axson, J. L., Diaz Martinez, M., Venero, I., Santos-Figueroa, G., Stokes, M. D., Deane, G. B., Mayol-Bracero, O. L., Grassian, V. H., Bertram, T. H., Bertram, A. K., Moffett, B. F., and Franc, G. D.: Sea spray aerosol as a unique source of ice nucleating particles, Proceedings of the National Academy of Sciences, 113, 5797–5803, https://doi.org/10.1073/pnas.1514034112, 2016.

Fenger, M., Sørensen, L. L., Kristensen, K., Jensen, B., Nguyen, Q. T., Nøjgaard, J. K., Massling, A., Skov, H., Becker, T., and Glasius, M.: Sources of anions in aerosols in northeast Greenland during late winter, Atmospheric Chemistry and Physics, 13, 1569–1578, https://doi.org/10.5194/acp-13-1569-2013, 2013.

Fletcher, N. H.: The physics of rainclouds, University Press, Cambridge, 1962.

Gong, X., Wex, H., van Pinxteren, M., Triesch, N., Fomba, K. W., Lubitz, J., Stolle, C., Robinson, T.-B., Müller, T., Herrmann, H., and Stratmann, F.: Characterization of aerosol particles at Cabo Verde close to sea level and at the cloud level – Part 2: Ice-nucleating particles in air, cloud and seawater, Atmospheric Chemistry and Physics, 20, 1451–1468, https://doi.org/10.5194/acp-20-1451-2020, 2020.

https://doi.org/10.5194/acp-2022-761
Preprint. Discussion started: 17 November 2022

Gong, X., Radenz, M., Wex, H., Seifert, P., Ataei, F., Henning, S., Baars, H., Barja, B., Ansmann, A., and Stratmann, F.: Significant continental source of ice-nucleating particles at the tip of Chile's southernmost Patagonia region, Atmospheric Chemistry and Physics Discussions, 2022, 1–29, https://doi.org/10.5194/acp-2022-71, 2022.

Griesche, H. J., Ohneiser, K., Seifert, P., Radenz, M., Engelmann, R., and Ansmann, A.: Contrasting ice formation in Arctic clouds: surface-coupled vs. surface-decoupled clouds, Atmospheric Chemistry and Physics, 21, 10 357–10 374, https://doi.org/10.5194/acp-21-10357-2021, 2021.

Gryning, S.-E., Batchvarova, E., Floors, R., Münkel, C., Sørensen, L., and Skov, H.: Observed aerosol-layer depth at Station Nord in the high Arctic, International Journal of Climatology, 2022.

Hande, L. B. and Hoose, C.: Partitioning the primary ice formation modes in large eddy simulations of mixed-phase clouds, Atmospheric Chemistry and Physics, 17, 14 105–14 118, https://doi.org/10.5194/acp-17-14105-2017, 2017.

Hartmann, M., Adachi, K., Eppers, O., Haas, C., Herber, A., Holzinger, R., Hühnerbein, A., Jäkel, E., Jentzsch, C., van Pinxteren, M., Wex, H., Willmes, S., and Stratmann, F.: Wintertime Airborne Measurements of Ice Nucleating Particles in the High Arctic: A Hint to a Marine, Biogenic Source for Ice Nucleating Particles, Geophysical Research Letters, 47, 1–11, https://doi.org/10.1029/2020gl087770, 2020.

Hartmann, M., Gong, X., Kecorius, S., van Pinxteren, M., Vogl, T., Welti, A., Wex, H., Zeppenfeld, S., Herrmann, H., Wiedensohler, A., and Stratmann, F.: Terrestrial or marine – indications towards the origin of ice-nucleating particles during melt season in the European Arctic up to 83.7° N, Atmospheric Chemistry and Physics, 21, 11 613–11 636, https://doi.org/10.5194/acp-21-11613-2021, 2021.

Hawker, R. E., Miltenberger, A. K., Wilkinson, J. M., Hill, A. A., Shipway, B. J., Cui, Z., Cotton, R. J., Carslaw, K. S., Field, P. R., and Murray, B. J.: The temperature dependence of ice-nucleating particle concentrations affects the radiative properties of tropical convective cloud systems, Atmospheric Chemistry and Physics, 21, 5439–5461, https://doi.org/10.5194/acp-21-5439-2021, 2021.

Hersbach, H., Bell, B., Berrisford, P., Biavati, G., Horányi, A., Muñoz Sabater, J., Nicolas, J., Peubey, C., Radu, R., Rozum, I., Schepers, D., Simmons, A., Soci, C., Dee, D., and Thépaut, J.-N.: ERA5 hourly data on single levels from 1979 to present. Copernicus Climate Change Service (C3S) Climate Data Store (CDS), https://doi.org/10.24381/cds.adbb2d47, accessed on 20-APR-2022, 2018.

Hill, T. C. J., DeMott, P. J., Tobo, Y., Fröhlich-Nowoisky, J., Moffett, B. F., Franc, G. D., and Kreidenweis, S. M.: Sources of organic ice nucleating particles in soils, Atmospheric Chemistry and Physics, 16, 7195–7211, https://doi.org/10.5194/acp-16-7195-2016, 2016.

Hoose, C. and Möhler, O.: Heterogeneous ice nucleation on atmospheric aerosols: a review of results from laboratory experiments, Atmospheric Chemistry and Physics, 12, 9817–9854, https://doi.org/10.5194/acp-12-9817-2012, 2012.

Hu, Y. X., Vaughan, M., Liu, Z. Y., Lin, B., Yang, P., Flittner, D., Hunt, B., Kuehn, R., Huang, J. P., Wu, D., Rodier, S., Powell, K., Trepte, C., and Winker, D.: The depolarization - attenuated backscatter relation: CALIPSO lidar measurements vs. theory, Optics Express, 15, 5327–5332, https://doi.org/10.1364/oe.15.005327, 2007.

Hu, Y. X., Winker, D., Vaughan, M., Lin, B., Omar, A., Trepte, C., Flittner, D., Yang, P., Nasiri, S. L., Baum, B., Sun, W. B., Liu, Z. Y., Wang, Z., Young, S., Stamnes, K., Huang, J. P., Kuehn, R., and Holz, R.: CALIPSO/CALIOP Cloud Phase Discrimination Algorithm, Journal of Atmospheric and Oceanic Technology, 26, 2293–2309, https://doi.org/10.1175/2009jtecha1280.1, 2009.

Intrieri, J., Fairall, C., Shupe, M., Persson, O., Andreas, E., Guest, P., and Moritz, R.: An annual cycle of Arctic surface cloud forcing at SHEBA, J. Geophys. Res, 107, https://doi.org/10.1029/2000jc000439, 2002.

Irish, V. E., Elizondo, P., Chen, J., Chou, C., Charette, J., Lizotte, M., Ladino, L. A., Wilson, T. W., Gosselin, M., Murray, B. J., Polishchuk, E., Abbatt, J. P. D., Miller, L. A., and Bertram, A. K.: Ice-nucleating particles in Canadian Arctic sea-surface microlayer and bulk seawater, Atmospheric Chemistry and Physics, 17, 10 583–10 595, https://doi.org/10.5194/acp-17-10583-2017, 2017.

Kanji, Z. A., Ladino, L. A., Wex, H., Boose, Y., Burkert-Kohn, M., Cziczo, D. J., and Krämer, M.: Overview of Ice Nucleating Particles, Meteorological Monographs, 58, 1.1–1.33, https://doi.org/10.1175/amsmonographs-d-16-0006.1, 2017.

Kirpes, R. M., Bonanno, D., May, N. W., Fraund, M., Barget, A. J., Moffet, R. C., Ault, A. P., and Pratt, K. A.: Wintertime Arctic Sea Spray Aerosol Composition Controlled by Sea Ice Lead Microbiology, ACS Central Science, 5, 1760–1767, https://doi.org/10.1021/acscentsci.9b00541, pmid: 31807677, 2019.

Lange, R., Dall'Osto, M., Skov, H., Nielsen, I., Beddows, D., Simo, R., Harrison, R., and Massling, A.: Characterization of distinct Arctic Aerosol Accumulation Modes and their Sources, Atmospheric Environment, 183, 1–10, https://doi.org/10.1016/j.atmosenv.2018.03.060, 2018.

Li, G., Wieder, J., Pasquier, J. T., Henneberger, J., and Kanji, Z. A.: Predicting atmospheric background number concentration of ice nucleating particles in the Arctic, Atmospheric Chemistry and Physics Discussions, 2022, 1–27, https://doi.org/10.5194/acp-2022-21, 2022.

Maki, L. R., Galyan, E. L., Chang-Chien, M.-M., and Caldwell, D. R.: Ice nucleation induced by pseudomonas syringae., Applied microbiology, 28 3, 456–9, https://doi.org/10.1128/am.28.3.456-459.1974, 1974.

Massling, A., Nielsen, I. E., Kristensen, D., Christensen, J. H., Sørensen, L. L., Jensen, B., Nguyen, Q. T., Nøjgaard, J. K., Glasius, M., and Skov, H.: Atmospheric black carbon and sulfate concentrations in Northeast Greenland, Atmospheric Chemistry and Physics, 15, 9681–9692, https://doi.org/10.5194/acp-15-9681-2015, 2015.

Maters, E. C., Dingwell, D. B., Cimarelli, C., Müller, D., Whale, T. F., and Murray, B. J.: The importance of crystalline phases in ice nucleation by volcanic ash, Atmospheric Chemistry and Physics, 19, 5451–5465, https://doi.org/10.5194/acp-19-5451-2019, 2019.

McCluskey, C. S., Hill, T. C. J., Malfatti, F., Sultana, C. M., Lee, C., Santander, M. V., Beall, C. M., Moore, K. A., Cornwell, G. C., Collins, D. B., Prather, K. A., Jayarathne, T., Stone, E. A., Azam, F., Kreidenweis, S. M., and DeMott, P. J.: A Dynamic Link between Ice Nucleating Particles Released in Nascent Sea Spray Aerosol and Oceanic Biological Activity during Two Mesocosm Experiments, Journal of the Atmospheric Sciences, 74, 151–166, https://doi.org/10.1175/jas-d-16-0087.1, 2017.

Morrison, H., De Boer, G., Feingold, G., Harrington, J., Shupe, M., and Sulia, K.: Resilience of persistent Arctic mixed-phase clouds, Nature Geoscience, 5, 11–17, https://doi.org/10.1038/ngeo1332, 2012.

Murray, B. J., O'Sullivan, D., Atkinson, J. D., and Webb, M. E.: Ice nucleation by particles immersed in supercooled cloud droplets, Chem. Soc. Rev., 41, 6519–6554, https://doi.org/10.1039/c2cs35200a, 2012.

Murray, B. J., Carslaw, K. S., and Field, P. R.: Opinion: Cloud-phase climate feedback and the importance of ice-nucleating particles, Atmospheric Chemistry and Physics, 21, 665–679, https://doi.org/10.5194/acp-21-665-2021, 2021.

Myhre, G., Lund Myhre, C., Samset, B. H., and Storelvmo, T.: Aerosols and their Relation to Global Climate and Climate Sensitivity, Nature Education Knowledge, 4, 7, 2013.

O'Sullivan, D., Murray, B. J., Malkin, T. L., Whale, T. F., Umo, N. S., Atkinson, J. D., Price, H. C., Baustian, K. J., Browse, J., and Webb, M. E.: Ice nucleation by fertile soil dusts: relative importance of mineral and biogenic components, Atmospheric Chemistry and Physics, 14, 1853–1867, https://doi.org/10.5194/acp-14-1853-2014, 2014.

O'Sullivan, D., Adams, M., Tarn, M., Harrison, A., Vergara-Temprado, J., Porter, G., Holden, M., Sanchez-Marroquin, A., Carotenuto, F., Whale, T., McQuaid, J., Walshaw, R., Hedges, D., Burke, I., Cui, Z., and Murray, B.: Contributions of biogenic material to the atmospheric ice-nucleating particle population in North Western Europe, Scientific Reports, 8, https://doi.org/10.1038/s41598-018-31981-7, 2018.

Ott, W.: A Physical Explanation of the LogNormality of Pollutant Concentrations, Journal of the Air & Waste Management Association, 40, 1378–83, https://doi.org/10.1080/10473289.1990.10466789, 1990.

https://doi.org/10.5194/acp-2022-761
Preprint. Discussion started: 17 November 2022

Atmospheric Chemistry and Physics Discussions

Petters, M. D. and Wright, T. P.: Revisiting ice nucleation from precipitation samples, Geophysical Research Letters, 42, 8758–8766, https://doi.org/10.1002/2015gl065733, 2015.

Petters, M. D., Parsons, M. T., Prenni, A. J., Demott, P. J., Kreidenweis, S. M., Carrico, C. M., Sullivan, A. P., McMeeking, G. R., Levin, E., Wold, C. E., Collett, J. L., and Moosmüller, H.: Ice nuclei emissions from biomass burning, Journal of Geophysical Research (Atmospheres), 114, D07209, https://doi.org/10.1029/2008jd011532, 2009.

Pithan, F. and Mauritsen, T.: Arctic amplification dominated by temperature feedbacks in contemporary climate models, Nature Geoscience, 7, https://doi.org/10.1038/ngeo2071, 2014.

Pruppacher, H. and Klett, J.: Microphysics of Clouds and Precipitation, vol. 18, https://doi.org/10.1007/978-0-306-48100-0, 2010.

Rantanen, M., Karpechko, A. Y., Lipponen, A., Nordling, K., Hyvärinen, O., Ruosteenoja, K., Vihma, T., and Laaksonen, A.: The Arctic has warmed nearly four times faster than the globe since 1979, Communications Earth & Environment, 3, 168, https://doi.org/10.1038/s43247-022-00498-3, 2022.

Sanchez-Marroquin, A., Arnalds, O., Baustian-Dorsi, K. J., Browse, J., Dagsson-Waldhauserova, P., Harrison, A. D., Maters, E. C., Pringle, K. J., Vergara-Temprado, J., Burke, I. T., McQuaid, J. B., Carslaw, K. S., and Murray, B. J.: Iceland is an episodic source of atmospheric ice-nucleating particles relevant for mixed-phase clouds, Science Advances, 6, eaba8137, https://doi.org/10.1126/sciadv.aba8137, 2020.

Schmale, J., Sharma, S., Decesari, S., Pernov, J., Massling, A., Hansson, H.-C., von Salzen, K., Skov, H., Andrews, E., Quinn, P. K., Upchurch, L. M., Eleftheriadis, K., and Traversi, R.: Pan-Arctic seasonal cycles and long-term trends of aerosol properties from ten observatories, Atmospheric Chemistry and Physics Discussions, 2021, 1–53, https://doi.org/10.5194/acp-2021-756, 2021.

Schnell, R. and Vali, G.: Biogenic Ice Nuclei: Part I. Terrestrial and Marine Sources, Journal of Atmospheric Sciences, 33, 1554–1564, https://doi.org/10.1175/1520-0469(1976)033<1554:binpit>2.0.co;2, 1976.

Schrod, J., Thomson, E. S., Weber, D., Kossmann, J., Pöhlker, C., Saturno, J., Ditas, F., Artaxo, P., Clouard, V., Saurel, J.-M., Ebert, M., Curtius, J., and Bingemer, H. G.: Long-term deposition and condensation ice-nucleating particle measurements from four stations across the globe, Atmospheric Chemistry and Physics, 20, 15 983–16 006, https://doi.org/10.5194/acp-20-15983-2020, 2020.

Schuur, E., McGuire, A., Schädel, C., Grosse, G., Harden, J., Hayes, D., Hugelius, G., Koven, C., Kuhry, P., Lawrence, D., Natali, S., Olefeldt, D., Romanovsky, V., Schaefer, K., Turetsky, M., Treat, C., and Vonk, J.: Climate change and the permafrost carbon feedback, Nature, 2015, 171–179, https://doi.org/10.1038/nature14338, 2015.

Serreze, M. C. and Barry, R. G.: Processes and impacts of Arctic amplification: A research synthesis, Global and Planetary Change, 77, 85–96, https://doi.org/10.1016/j.gloplacha.2011.03.004, 2011.

Shupe, M. D. and Intrieri, J. M.: Cloud Radiative Forcing of the Arctic Surface: The Influence of Cloud Properties, Surface Albedo, and Solar Zenith Angle, Journal of Climate, 17, 616–628, https://doi.org/10.1175/1520-0442(2004)017<0616:crfota>2.0.co;2, 2004.

Shupe, M. D., Matrosov, S. Y., and Uttal, T.: Arctic Mixed-Phase Cloud Properties Derived from Surface-Based Sensors at SHEBA, Journal of the Atmospheric Sciences, 63, 697–711, https://doi.org/10.1175/jas3659.1, 2006.

Shupe, M. D., Rex, M., Blomquist, B., Persson, P. O. G., Schmale, J., Uttal, T., et al.: Overview of the MOSAiC expedition - Atmosphere, Elementa Science of the Anthropocene, 10, https://doi.org/10.1525/elementa.2021.00060, 2022.

Si, M., Irish, V. E., Mason, R. H., Vergara-Temprado, J., Hanna, S. J., Ladino, L. A., Yakobi-Hancock, J. D., Schiller, C. L., Wentzell, J. J. B., Abbatt, J. P. D., Carslaw, K. S., Murray, B. J., and Bertram, A. K.: Ice-nucleating ability of aerosol particles and possible sources at three coastal marine sites, Atmospheric Chemistry and Physics, 18, 15 669–15 685, https://doi.org/10.5194/acp-18-15669-2018, 2018.

Spreen, G., Kaleschke, L., and Heygster, G.: Sea ice remote sensing using AMSR-E 89-GHz channels, Journal of Geophysical Research, 113, C02s03, https://doi.org/10.1029/2005jc003384, 2008.

Stein, A. F., Draxler, R. R., Rolph, G. D., Stunder, B. J. B., Cohen, M. D., and Ngan, F.: NOAA's HYSPLIT Atmospheric Transport and Dispersion Modeling System, Bulletin of the American Meteorological Society, 96, 2059–2077, https://doi.org/10.1175/bams-d-14-00110.1, 2015.

Szyrmer, W. and Zawadzki, I.: Biogenic and Anthropogenic Sources of Ice-Forming Nuclei: A Review, Bulletin of the American Meteorological Society, 78, 209–228, https://doi.org/10.1175/1520-0477(1997)078<0209:baasoi>2.0.co;2, 1997.

Tan, I., Barahona, D., and Coopman, Q.: Potential Link Between Ice Nucleation and Climate Model Spread in Arctic Amplification, Geophysical Research Letters, 49, https://doi.org/10.1029/2021gl097373, 2022.

Tobo, Y., Adachi, K., DeMott, P., Hill, T., Hamilton, D., Mahowald, N., Nagatsuka, N., Ohata, S., Uetake, J., Kondo, Y., and Koike, M.: Glacially sourced dust as a potentially significant source of ice nucleating particles, Nature Geoscience, 12, 1–6, https://doi.org/10.1038/s41561-019-0314-x, 2019.

Vali, G., DeMott, P. J., Möhler, O., and Whale, T. F.: Technical Note: A proposal for ice nucleation terminology, Atmospheric Chemistry and Physics, 15, 10 263–10 270, https://doi.org/10.5194/acp-15-10263-2015, 2015.

Vavrus, S. J., Bhatt, U. S., and Alexeev, V. A.: Factors Influencing Simulated Changes in Future Arctic Cloudiness, Journal of Climate, 24, 4817–4830, https://doi.org/10.1175/2011jcli4029.1, 2011.

Villanueva, D., Senf, F., and Tegen, I.: Hemispheric and Seasonal Contrast in Cloud Thermodynamic Phase From A-Train Spaceborne Instruments, Journal of Geophysical Research-Atmospheres, 126, https://doi.org/10.1029/2020jd034322, 2021.

Welti, A., Müller, K., Fleming, Z. L., and Stratmann, F.: Concentration and variability of ice nuclei in the subtropical maritime boundary layer, Atmospheric Chemistry and Physics, 18, 5307–5320, https://doi.org/10.5194/acp-18-5307-2018, 2018.

Wendisch, M., Brückner, M., Burrows, J. P., Crewell, S., Dethloff, K., Ebell, K., Lüpkes, C., Macke, A., Notholt, J., Quaas, J., Rinke, A., and Tegen, I.: Understanding Causes and Effects of Rapid Warming in the Arctic, Eos, 98, https://doi.org/10.1029/2017eo064803, 2017.

Wex, H., Huang, L., Zhang, W., Hung, H., Traversi, R., Becagli, S., Sheesley, R. J., Moffett, C. E., Barrett, T. E., Bossi, R., Skov, H., Hünerbein, A., Lubitz, J., Löffler, M., Linke, O., Hartmann, M., Herenz, P., and Stratmann, F.: Annual variability of ice-nucleating particle concentrations at different Arctic locations, Atmospheric Chemistry and Physics, 19, 5293–5311, https://doi.org/10.5194/acp-19-5293-2019, 2019.

Wild, B., Andersson, A., Bröder, L., Vonk, J., Hugelius, G., McClelland, J. W., Song, W., Raymond, P. A., and Gustafsson, Ö.: Rivers across the Siberian Arctic unearth the patterns of carbon release from thawing permafrost, Proceedings of the National Academy of Sciences, 116, 10 280–10 285, https://doi.org/10.1073/pnas.1811797116, 2019.

Wilson, T., Ladino, L., Alpert, P., Breckels, M., Brooks, I., Browse, J., Burrows, S., Carslaw, K., Huffman, J., Judd, C., Kilthau, W., Mason, R., Mcfiggans, G., Miller, L., Nájera, J., Polishchuk, E., Rae, S., Schiller, C., Si, M., and Murray, B.: A marine biogenic source of atmospheric ice-nucleating particles, Nature, 525, 234, https://doi.org/10.1038/nature14986, 2015.

Zeppenfeld, S., Van Pinxteren (née Schellin), M., Hartmann, M., Bracher, A., Stratmann, F., and Herrmann, H.: Glucose as a Potential Chemical Marker for Ice Nucleating Activity in Arctic Seawater and Melt Pond Samples, Environmental Science & Technology, 53, https://doi.org/10.1021/acs.est.9b01469, 2019.

Šantl Temkiv, T., Lange, R., Beddows, D., Rauter, U., Pilgaard, S., Dall'Osto, M., Gunde-Cimerman, N., Massling, A., and Wex, H.: Biogenic Sources of Ice Nucleating Particles at the High Arctic Site Villum Research Station, Environmental Science & Technology, 53, 10 580–10 590, https://doi.org/10.1021/acs.est.9b00991, pmid: 31094516, 2019.